CHAPTER 6

ON-OFF CONTROL BASED MPPT AND RELIABILITY ASPECT OF DFIG DRIVEN BY WT

6.1 Introduction

Up to the present stage, the mainstream of electrical energy has generated from conventional vestige sources, which are predominantly non-renewable sources such as gas, oil, and coal. This type of energy conversion emits an enormous amount of carbon dioxide to the surroundings, which outcome cause global warming. The advanced electricity generation technologies, the renewable energy converters are admirably glowing on their smaller size, lower cost per unit. Alternatively, refers to fuel source′s limitations and the insane price of thermal plants generated electricity per kW connected with the variable cost of fuel cause a global trend to replace limited energy sources with plentiful alternatives. Wind power is the best renewable energy sources which have extensively developed in recent years; Wind power has several advantages such as no pollution, the comparatively low capital cost involved and the short gestation period [1]. According to the WGEC 2010 annual report, wind energy has developed as well as used in more than 70 countries. Large-scale wind power consumption annual expansion rate was 24.6% in 2009. This rate dropped by 0.5% in 2010 because of financial calamity; the plunge could be more terrible if China had not introduced as a new prototype to the field of wind energy. While the US installed 50% less in 2010 compared with 2009 and the Europe market was down by 7.5%, China owned approximately half of the global mechanism, with the amount of 18.9 GW. This large installation preserved the global enhance the rate at 24.1% and yielded 195 GW, which was about twice of 94.19 GW that installed in late 2007. There were numerous types of

generators for wind energy converters application. A various kind of generator in the older time was synchronous generators whereas, by manufacturing technology improvements, induction generators of different types become additional accepted in wind energy conversion field. Induction generators, mainly doubly fed induction generators are attractive more and more popular in renewable source employment [2]. Elementary induction generators have a few weaknesses such as reactive power utilization and unregulated voltage profile during variable rotor speed. These problems can solve by execution of DFIG along with power electronic converter or regulators. This manuscript is an overview and conclusion on the last one decade's research, which has done associated with DFIG controllers, their impact on power networks and vice versa. The power output of the wind generator may fluctuate due to variations in the wind speed. Efforts have been made to estimate wind speed a priori from statistical data [3, 4]. Utilize of probabilistic methods to catch out a power output of a wind generator system as described in [5]. The pitch control method and sophisticated gear trains convey the generator rotor speed near to the synchronous speed in a limited speed range. Due to modern control techniques together with power electronics and drives, the real, as well as reactive power output of the wind generator, can track their reference values correctly despite the speed variations. The DFIG with the fully controlled serial converter on rotor side has become admired as a wind-driven a generator for high power approach.

The chapter includes Introduction in section I. Section II involves an overview and theoretical concepts of the wind energy conversion systems for wind turbine systems. Part III contains ideas of the Wind Energy generating system as well as a doubly fed induction generator. Section IV incorporates the Methodology being followed in implementing the models of on-off control based MPPT along with MPPT concept and methods as well as MPPT controllers and

their MPPT type's technique with on-off control. Section V gives the brief operation of the whole system, how each of the blocks performs to achieve the desired objective and results of the simulation are presented with the analysis of the obtained result. In section VI and VII, the stationary Markov process is used to compute the reliability of the whole DFIG based WT scheme and sub-systems. The conclusion has been described in Section VIII.

6.2 Wind Energy Generating Systems

Wind turbines produce electricity by using the power of the wind to drive an electrical generator Passing the blades, the wind generates pick up plus exerts a turning force. The revolving blades turn a shaft inside the nacelle, which goes into a gearbox. The gearbox adjusts the rotating speed to that which is suitable intended to the generator, which uses magnetic fields to exchange the rotating energy into electrical energy. The basic block of WECS is shown in Figure (6.1).

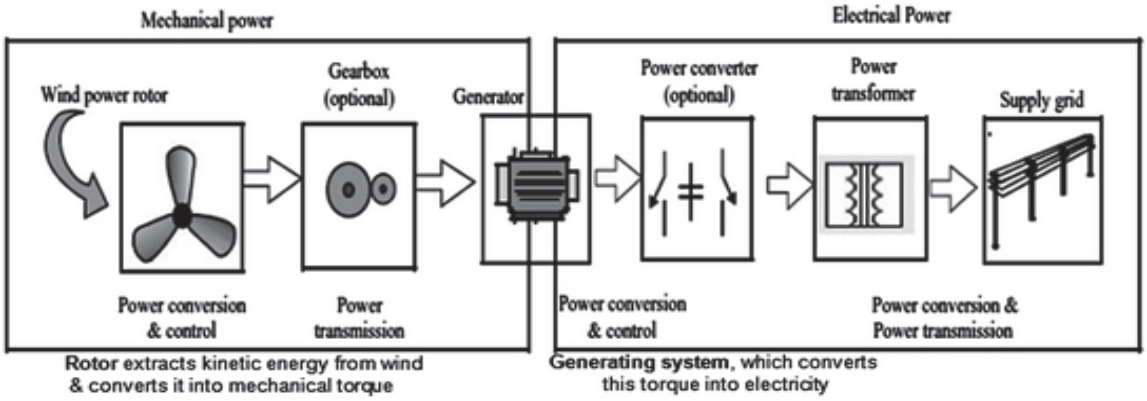

Figure 6.1: Basic Block of WECS

The power production goes to a transformer, which converts the electricity from the generator at approximately 700V to the suitable voltage for the electrical power collection system, usually 33 kV [150]. The wind turbine takes out kinetic energy from the swept area of the blades. The power comprised in the wind is given by the kinetic energy of the flowing air mass per unit time. That is

$$P_{air} = \frac{1}{2}\rho\pi R^2 v^3 \tag{1}$$

Where P_{air} is the power contained in the wind (in watts), ρ is the air density (1.225 kg/m^3 at 15°C and standard pressure), R is the blade radius of the wind turbine, and *v* is the wind velocity without rotor disturbance. i.e., preferably at an infinite distance from the rotor (in meter per second). Even though the above equation gives the power accessible in the wind, the power transfer to the wind turbine rotor is concentrated by the power coefficient, C_p.

$$C_p = \frac{P_{windTurbine}}{P_{air}} \tag{2}$$

On the other hand the P_{air} is converted in to mechanical power by C_p as given below.

$$P_m = \frac{1}{2}\rho\pi R^2 v^3 C_p(\lambda,\beta) \tag{3}$$

Here, R is the radius of the blade of a wind turbine ρ is the air mass density, *v* is the wind speed, λ is the tip speed ratio, β is the pitch angle, C_p is the wind turbine energy coefficient. The maximum value of C_p is determined by the Betz limit, which states a turbine can not extract more than 59.3% of the power from the air stream. In reality, wind turbine rotors have maximum C_p values in the range 25-45%. Several numerical approximations exist for $C_p(\lambda,\beta)$ [151].

On another hand, the Specified Rated capacity (SRC) is an important index which is used to compare a variety of wind turbine designs in [152] is formulate as follows.

$$SRC = \frac{GeneratorPowerRating}{RotorSweptArea} \tag{4}$$

It varies between from 0.2 (for small rotors) to 0.6 (large rotors).

6.2.1 Aerodynamic Power Conversion and Control: The aerodynamic power conversion involves the wind turbine blade design and its operation to harness the mechanical power within

certain wind velocity. The aerodynamic power conversion includes the interaction of air flow to create drag force (F_D) and lift force (F_L). Where is the pitch angle, β, is the angle between the chord line of the blade and the plane of rotation. The angle of attack, κ, is the angle between chord line of the blade and relative wind direction [153,154]. It can be understood from Figure (6.2).

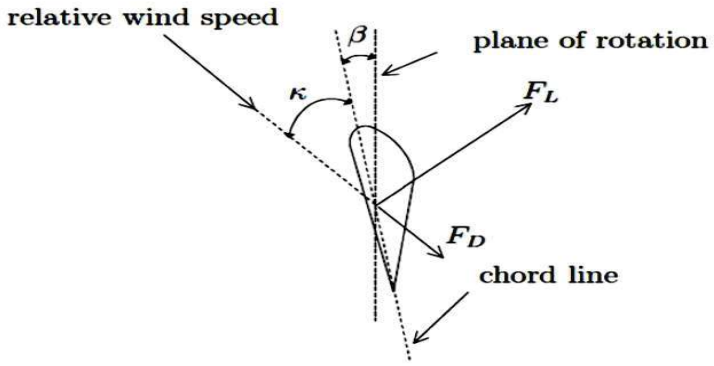

Figure 6.2: Pitch Angle and Angle of Attack

The power extract from the wind is given as a fraction of the total power in the wind. The portion is described by a coefficient of performance, C_p [153]. The power coefficient determines the power to be extracted for a given wind velocity. At the high wind speed, it is essential to limit the input power to the turbine, i.e., aerodynamic power control. There is three primary behavior of performing the aerodynamic power control, i.e., through stall, pitch or active stall control. Stall control involves that the blades are designed to stall in high wind speeds, and no pitch mechanism is thus required [155].The pitch control can be used to maximize the power output from the turbine by changing the pitch angle. At higher wind speeds, the pitch angle is controlled to decrease the angle of attack which reduces aerodynamic power extracted [155]. The control of pitch angle to maximize the power is beyond the scope of the thesis. Therefore, only tip speed ratio, i.e., generator speed is controlled to achieve the maximum output power.

6.2.2 Power Coefficient (C_p)

The ratio of power output of the machine to the power contained in the wind is called as power coefficient (Cp). i.e. $C_p = \frac{P_{windTurbine}}{P_{air}}$, whereas the $C_p(\lambda,\beta)$ is given as below;

$$C_p(\lambda,\beta) = 0.22\left(\frac{116}{\lambda_i} - 0.4\beta - 5\right)e^{\frac{-12.5}{\lambda_i}} \text{ Where; } \frac{1}{\lambda_i} = \frac{1}{\lambda + 0.08\beta} - \frac{0.035}{\beta^3 + 1}$$

On the other hand theTip Speed Ratio (TSR) is the ratio of the wind flowing from the tip of the blade to the wind velocity is known as Tip speed ratio (λ) i.e. $\lambda = \frac{\omega_t r}{v_\omega}$ and Pitch Angle β is the angle between the chord of aerofoil section and the plane of revolution. Equation $P_m = \frac{1}{2}\rho\pi R^2 v^3 C_p(\lambda,\beta)$ gives the mechanical power extracted from the turbine. The variation of power coefficient (C_p) according to tip speed ratio (λ) is shown in Figure (6.3) [156].

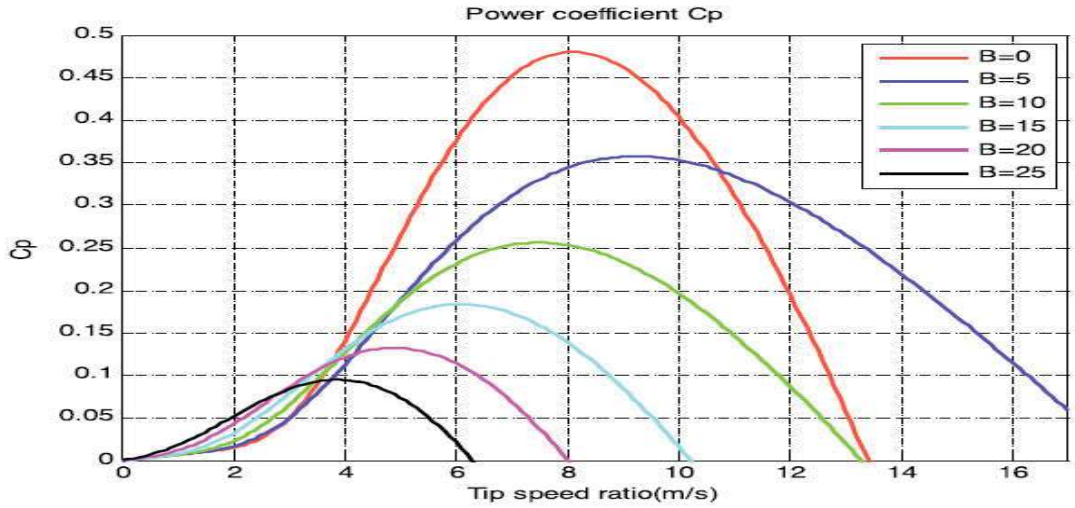

Figure 6.3: C_p Vs. λ

C_p can be computed either by measurements or by theoretical computations. Based on theoretical calculations, the empirical relation of C_p has been derived in [157] and [158]. In [157], the observed relationship of C_p as a function of tip speed (λ) and pitch angle (β) has been given. As the pitch angle control is not studied in this thesis work, here β has been taken 45 degrees.

6.3 Doubly Fed Induction Generator based Wind Turbine System

The DFIG wind turbines are more and more used in generally find farms. A typical DFIG scheme is exposed in Figure(6.4). The AC/DC/AC converter comprises of two apparatus: the rotor side converter C_{rotor} as well as a Grid side converter C_{grid}. These converters are voltage source converters that employ forced commutation power electronic devices (IGBTS) to synthesize AC voltage from DC voltage source. A capacitor linked on DC side acts as a DC voltage source. The generator slip rings are connected to the rotor side converter, which aids a DC link with the grid side converter in such a manner so-called back-to-back arrangement. The wind power captured by the turbine is transformed into electrical energy by the IG and is transferred to the grid by stator and rotor windings. The control system gives the pitch angle command, and the voltage controls for C_{rotor} as well as C_{grid} to control the power of the wind turbine, DC bus voltage and reactive power or voltage at grid terminals [143]. The DFIG based WT scheme is shown in Figure (6.4).

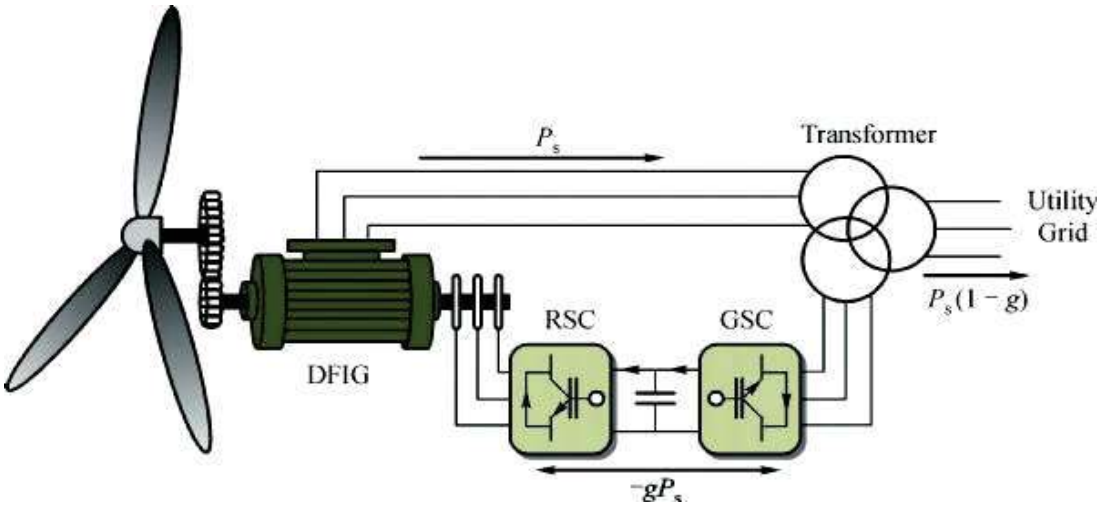

Figure 6.4: A DFIG based Wind turbine system

6.3.1 Operation: while the rotor speed is larger than the revolving magnetic field from the stator, the stator induces a high current in the rotor. The quicker the rotor rotates, the more power

will be transferred as an electromagnetic force to the stator, and in turn transformed into electricity which is fed to the electric grid. The speed of a synchronous generator will differ with the rotational force functional to it. Its dissimilarity from synchronous speed in percent is called generator's slip. With rotor winding short-circuited, the generator at full load is only a small number of percent. With the DFIG, slip control is an offer by the rotor and grid side converters. At high rotor speeds, the slip power is improved and deliver to the grid, resultant in high on the whole system efficiency. If the rotor speed range is imperfect, the ratings of the frequency converters will be small compared to the generator rating, which helps in reducing converter losses and the system cost [156].Since the mechanical torque functional to the rotor is active for power generation and since the rotating speed of the magnetic flux in the air gap of the generator is active and steady for a constant frequency grid voltage, the sign of the rotor electric power output is a function of the slip sign. C_{rotor} and C_{grid} can generate or engrossing reactive power and be able to be used for controlling the reactive power or the network terminal voltage. The pitch angle is controlled to limit the generator output power to its standard value for high wind speeds. The network offers the necessary reactive power to the generator.

6.3.2 DFIG model: The model of the doubly fed induction generator is given by the following set of equations; Equations of stator voltage components [156]:

$$v_{ds} = R_s i_{ds} + \frac{d\varphi_{ds}}{dt} - w_s \varphi_{qs} \tag{5}$$

$$v_{qs} = R_s i_{qs} + \frac{d\varphi_{qs}}{dt} - w_s \varphi_{ds} \tag{6}$$

Equations of rotor voltage components:

$$v_{dr} = R_r i_{dr} + \frac{d\varphi_{dr}}{dt} - w_r \varphi_{qr} \quad (7)$$

$$v_{qr} = R_r i_{qr} + \frac{d\varphi_{qr}}{dt} - w_r \varphi_{dr} \quad (8)$$

Equations of stator flux components:

$$\varphi_{ds} = L_s i_{ds} + M i_{dr} \quad (9)$$

$$\varphi_{qs} = L_s i_{qs} + M i_{qr} \quad (10)$$

Equations of rotor flux components:

$$\varphi_{dr} = L_r i_{dr} + M i_{ds} \quad (11)$$

$$\varphi_{qr} = L_r i_{qr} + M i_{qs} \quad (12)$$

Equations of electromagnetic torque:

$$T_{em} = \frac{3}{2} P \left(\varphi_{ds} i_{qr} - \varphi_{ds} i_{dr} \right) \quad (13)$$

Mechanical equation:

$$T_{em} = T_r + J \frac{d\Omega}{dt} + f\Omega \quad (14)$$

Where as the active and reactive powers at the stator side and at the rotor side is defined as

$$P_s = \frac{3}{2}\left(v_{ds} i_{qs} + v_{qs} i_{ds} \right)$$
$$Q_s = \frac{3}{2}\left(v_{qs} i_{ds} - v_{ds} i_{qs} \right) \quad (15)$$

$$P_r = \frac{3}{2}\left(v_{dr} i_{qr} + v_{qr} i_{dr} \right)$$
$$Q_r = \frac{3}{2}\left(v_{qr} i_{dr} - v_{dr} i_{qr} \right) \quad (16)$$

Where, V_{ds}, v_{qs}, v_{dr}, v_{qr} represent the measured stator and rotor voltages components; i_{ds}, i_{qs}, i_{dr}, i_{qr} are respectively the elements of the stator and rotor currents. While $\varphi_{ds},\varphi_{qs},\varphi_{dr},\varphi_{qr}$ are the components of the stator and rotor flux vectors; R_s, R_r is the stator and rotor phase resistances; L_s, L_r are the cyclic stator and rotor inductances; p is pole pairs number; M is the cyclic mutual inductance; T_r is the load torque; f is the friction constant; J is the moment of inertia; w_r is the synchronous rotor speed; Ω is the mechanical rotor speed. And T_{em} is the electromagnetic torque. The wind turbine is used for the production of high power generators. The stator resistance of the DFIG is neglected, and the stator flux ϕ_s is set aligned with the d-axis and assumed to be constant [156].

Then, one can write $\phi_{ds} = \phi_s$ and $\varphi_{qs} = 0$. Consequently, Equations 21- 26, become respectively:

$$v_{ds} \approx 0 \tag{17}$$

$$v_s = v_{qs} \approx w_s \phi_s \tag{18}$$

$$\varphi_s = L_s i_{ds} + M i_{dr} \tag{19}$$

$$0 = L_s i_{qs} + M i_{qr} \tag{20}$$

$$v_{dr} = R_r i_{dr} + (Lr - \frac{M^2}{L_s}) \frac{di_{dr}}{dt} - g w_s (Lr - \frac{M^2}{L_s}) i_{qr} \tag{21}$$

$$v_{qr} = R_r i_{qr} + (Lr - \frac{M^2}{L_s}) \frac{di_{qr}}{dt} - g w_s (Lr - \frac{M^2}{L_s}) i_{dr} + g \frac{M_{vs}}{L_s} \tag{22}$$

Equations (17), (18), (19) and (20) are used to rewrite the stator active and reactive powers as follow: [156].

$$\begin{aligned} P_s &= -\frac{3Mv_s}{2L_s} i_{qr} \\ Q_s &= \frac{3v_s}{2L_s w_s}(v_s - M w_s i_{dr}) \end{aligned} \tag{23}$$

Moreover, the electromagnetic torque is given by:

$$T_{em} = -\frac{3}{2} P \frac{M}{L_s} \phi_s i_{qr} \tag{24}$$

Where v_s is the stator voltage magnitude assumed to be constant, w_s Synchronous angular speed.

6.4 Maximum PowerPoint Tracking Concept and Methods

At a given wind velocity, the mechanical power available from a wind turbine is a function of shaft speed. Capitalize on the power captured from the wind; the shaft speed has to be controlled by a variable-speed method. The wind turbine mechanical output power, P_T is affected by the ratio of the turbine shaft velocity and the wind velocity, i.e., tip-speed-ratio ($\lambda=R.\omega_r/v$). As a result of variations in wind speed, the turbine shaft speed ω_r (or generator shaft speed ω_g), and wind turbine power P_T will change. Figure (6.5) shows a family of typical P_T versus ω_r curves for different wind velocities for a standard system, as seen in this Figure [160]. Various power curves have different maximum power, P_{max} (or optimal power, P_{opt}) [159].

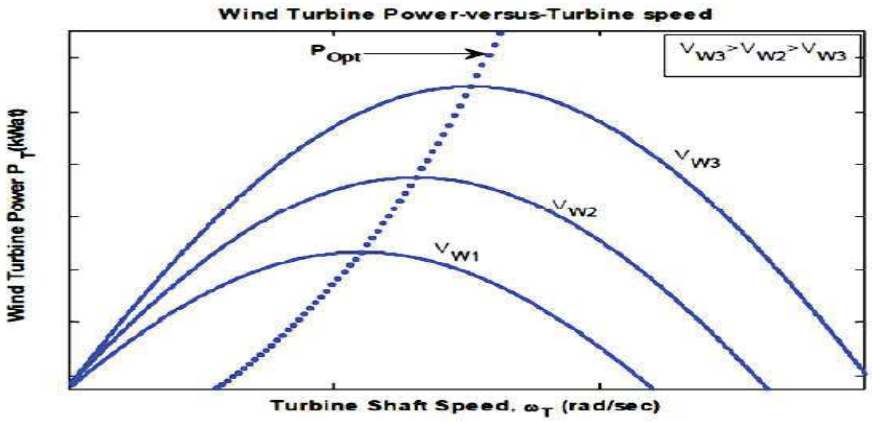

Figure 6.5: Maximum PowerPoint Tracking

6.4.1 Various kinds of MPPT Control techniques

Maximum power point tracking is an efficient method of extracting generated power from generating systems used by grid-connected inverters, solar battery chargers, and wind energy

conversion system. Wind power is dependent on weather, topology, and environment. It is essential to choose the best place where the quality of air can produce more electricity. Then it's hard to wind turbine to provide 60% of power from wind speed. Wind energy conversion system also has other losses similar to mechanical resistance and small generator efficiency. So the total output power from WECS depends to tracked wind power. Therefore, a maximum power point tracking control is required. [161].the various Types of MPPT control techniques are described as follows:

6.4.1.1 Tip Speed Ratio (TSR) Control

The optimal TSR is constant for a given wind turbine irrespective of variable wind speed as shown in Figure (6.6). When the wind turbine operates at this optimal TSR, the power so extracted from the WECS is maximized. Hence MPPT method forces the energy conversion system to perform at optimized TSR by comparing it with the actual value and supplying this error to the MPPT controller. The system responds by changing the generator speed to reduce this error. This optimized TSR can be computed experimentally and used as a reference. Though this method is simple as wind speed is measured directly, a precise measurement of wind speed is not possible and also the cost of the system increases. The block diagram of the tip speed ratio for MPPT control method is as shown in Figure (6.6) [162]. And Plot of Power coefficient vs. Tip speed ratio [162] is shown in Figure (6.7).

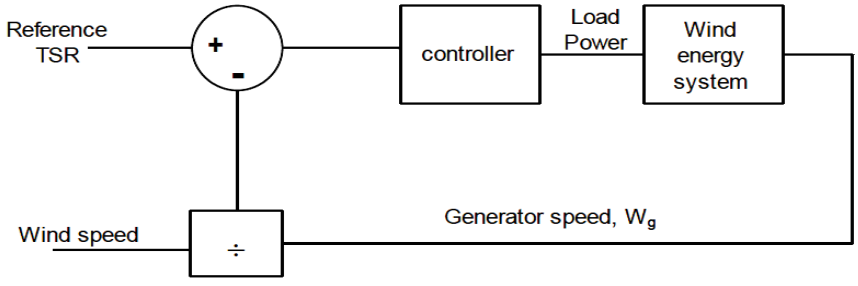

Figure 6.6: Block diagram for Tip speed ratio MPPT control

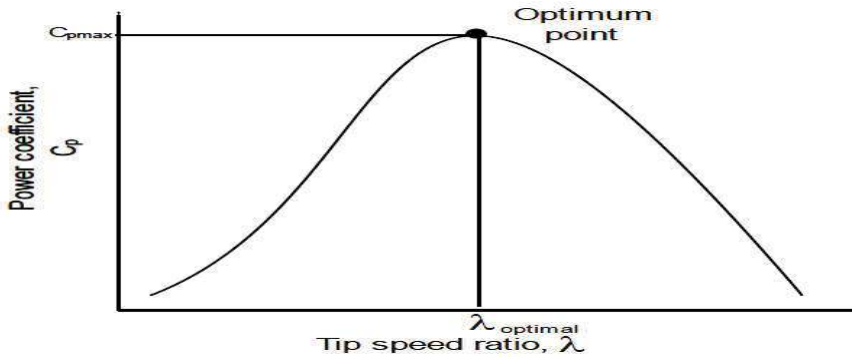

Figure 6.7: Plot of Power coefficient vs. Tip speed ratio

6.4.1.2 Optimal Torque Control (OT): As discussed in TSR MPPT method of control, maintaining the operation of the system at optimized TSR ensures maximum conversion of the available wind energy into mechanical energy. It can be seen from Figure (6.8) that the objective of this method is to adjust the PMSG torque about maximum power reference torque of the wind turbine at a given wind speed. The turbine power as a function of λ and w_r is determined mathematically. The block diagram as shown in Figure (6.8) describes the working of the OT controller [161].

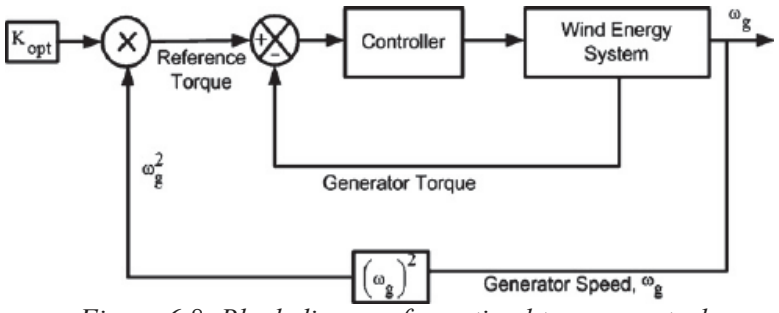

Figure 6.8: Block diagram for optimal torque control

6.4.1.3 Power Signal Feedback Control (PSF): In this controlling method, the reference optimum power curve of the wind turbine is obtained first from the experimental results. The operating points for maximum output power and the corresponding wind turbine speed are saved in a lookup table. The block diagram of the power signal feedback control is shown in Figure (6.9) [162].

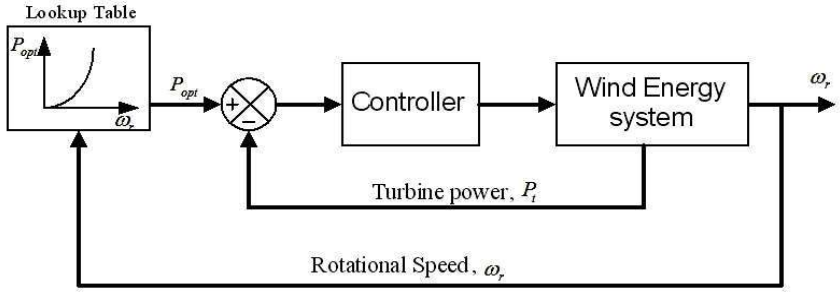

Figure 6.9: Block diagram for PSF MPPT control

6.4.1.4 Mechanical Speed-Sensor less PSF control: This method has the capability of providing a power reference for the controller analogous to maximum power point without measuring the turbine shaft speed. In other words, the method is based on PSF control, but neither wind velocity sensor nor turbine speed sensors are required. That is the significant advantage of this approach. The process can be developed for all wind turbine system including an induction generator (IG) [159].Figure (6.10) illustrates the block diagram of a mechanical speed-sensor less PSF control system [160]. In this method, a look-up table containing induction generator synchronous speeds (ω_s) corresponding to the optimal generator powers ($P_{gen\text{-}opt}$) is used. As the wind velocity keeps changing with time, the wind turbine must keep adjusting its speed to track the optimum wind turbine speed.

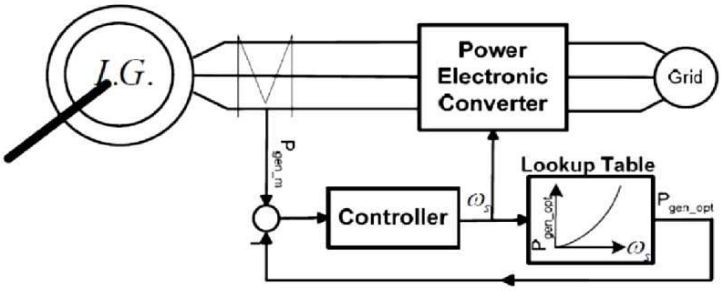

Figure 6.10: Mechanical speed-sensors less PSF control

6.4.1.5 Perturbation and observation control (P&O): The perturbation and observation method of control is an efficient optimization method which uses the principle of searching for

the local optimum point of a given function. It is used to examine the optimal operating point, and hence it will help to maximize the extracted energy. This control technique is based on introducing a small step size variation in a control variable and observing the changes in the target function till the slope of the function becomes zero. As shown in Figure (6.11) [162], the controller guides the operating point by locating the position and the distance of the functioning point from the peak point. The operating point moves towards the right if it is on extreme left side and vice versa. In this process, the duty cycle of the boost converter is perturbed, and the dc link power is observed. In this method, wind speed measurement is not required hence the mechanical sensors are not used. Therefore, this method of control is more reliable and cost-efficient [161].

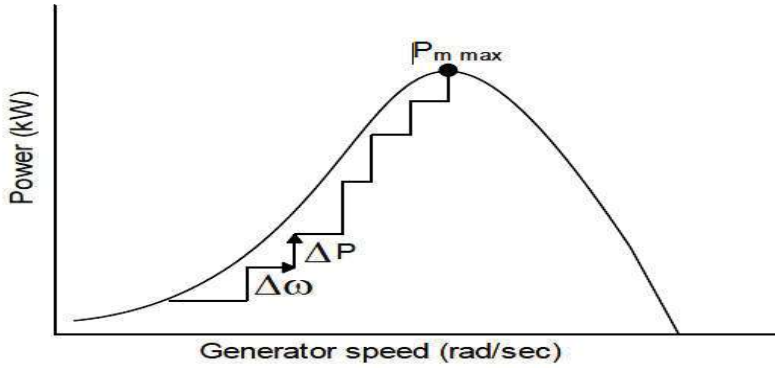

Figure 6.11: Plot of generated power in KW vs. generator speed in rad/sec

6.4.1.6 Wind Speed Measurement control

The wind turbine speed control aims to maintain wind turbine shaft speed at an optimal value, i.e., ω_{Pmax}, so that maximum mechanical power can be captured at any given wind velocity (V_W). In the wind speed measurement (WSM) method, both wind speed and shaft speed (ω_T) should be measured. Also, optimal tip-speed-ratio (λ_{opt}) must be determined by the controller. Figure (6.12) shows the wind speed measurement method [160].

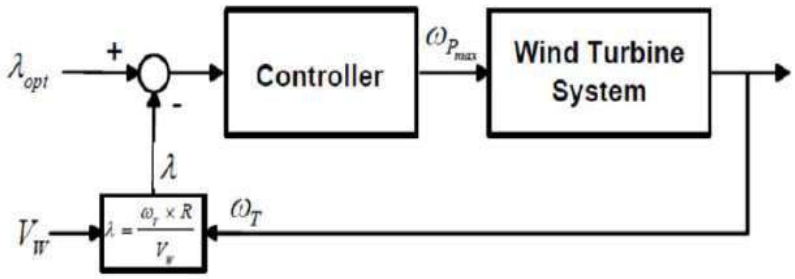

Figure 6.12: Wind speed measurement method

6.4.2 MPPT based On-Off Control technique for DFIG Systems

Several research works have been presented with different power/voltage control of DFIG based wind energy conversion system associated to the grid. These control diagrams are based on vector control notion with conventional PI controllers [162]. Fuzzy logic and adaptive fuzzy controllers have also been used in the power/voltage control loop [163]. Traditional controllers for wind energy conversion systems (WECS) can be developed for more well-organized strategies based on intelligent control technique. On-Off control is a robust scheme aiming at captured power maximisation of DFIG-based WECS connected to the grid. This approach superposes the tracking of the optimal torque value [43]. The control objective can be formulated as an optimization problem, in which an objective function is maximized or minimized, to extract the maximum power from the wind energy. There is a particular difficulty about the On-Off control, concerning the meaning of a switched module (follow the sign of the tip speed ratio inaccuracy) with guaranteed properties of attractiveness and stability. On-Off Control is based on maximum power point tracking method which is anticipated to control the rotor side converter of wind turbine equipped using the DFIG connected to the grid.

6.4.2.1 Controller Design

This approach supposes that the WECS reacts sufficiently fast to the variation of the low-frequency wind speed; this happens in the case of low-power WECS. Thus, for ensuring the

optimal energy conversion, it is sufficient to feed the electrical generator with the torque control value corresponding to the steady-state operating point. To this end, an on-off-controller-based structure can be used to zero the difference $\sigma = \lambda_{opt} - \lambda$, where λ is given by the low-frequency component of the wind speed *v* [43].

$$\lambda = \frac{\omega_r R}{v} \tag{25}$$

6.4.2.2 Rotor side converter based On-Off control

From Equation (24), the electromagnetic torque can be controlled directly by acting current component. Then; the rotor current is given by:

$$\mathrm{I_{q\_ref}} = -\frac{2L_s w_s}{3pv_s \mathrm{M}} \mathrm{T_{emref}} \tag{26}$$

From Equation (23), the stator reactive power can be controlled by acting on I_{dr}. Then, the d-reference rotor current is given by:

$$\mathrm{I_{qr\_ref}} = \frac{2L_s}{3v_s M}\left(\frac{3v_s^2}{2L_s w_s} - Q_{sref}\right) \tag{27}$$

For ensuring the maximum power point tracking an On-Off supposes that the WECS reacts sufficiently fast to the variation of wind speed as shown in Figure (6.13). An On-Off controller can be used to zero the difference between the optimal tip speed ratio and the actual tip speed ratio σ [164]:

$$\sigma = \lambda_{opt} - \lambda \tag{28}$$

The on-off objective is to make the difference between the optimal tip speed ratio and the actual tip speed ratio as small as possible with regulating the rotor speed according to the wind speed.

The control law u has two components:

$$\mathrm{T_{emref}} = \mathrm{u^{eq}} + \mathrm{u^{n}} \tag{29}$$

Where the equivalents control u^{eq} as defined:

$$u^{eq} = 0.5\pi \rho R^3 \frac{C_p(\lambda_{opt})}{i\lambda_{opt}} v_s^2 = A v_s^2 \quad (30)$$

With: $A = 0.5\pi \rho R^3 \frac{C_p(\lambda_{opt})}{i\lambda_{opt}}$ and i is the gear box ratio, u^n is an alternate, high-frequency component, which switches between two values, -α and +α, α>0:

$$u^n = \alpha \, \text{sign}(\sigma) \quad (31)$$

Component u^{eq} makes the system operated at the optimal point, whereas u^n has the role of stabilizing the system behavior around this point, once reached. The control law associated with the diagram in Figure (6.13) provides the steady state torque reference. The control input has, in this case, a large spectrum; the zero-order sample-and-hold (S&H in Figure (6.13)) has been introduced to limit the loop switching frequency. If this frequency is too large, the control circuit becomes inefficient. The zero order S&H element is approximated as a first order low-pass filter with a time constant $T_{S\&H} = T_s/2$, where T_s is the sampling period of the S&H. In Figure (6.13) the nonlinear part consists of an On-Off relay ("sign" block). The control of the rotor side converter is illustrated in Figure (6.13); the reference i_{qref} is derived from the high-speed shaft Ω_h and measured wind speed v by tuning the On-Off controller based maximum power point tracking (MPPT). Also, a current command i_{dref} is derived from Equation (23) to control the reactive power to the required value, as shown in Figure (6.13). Elsewhere; Equations (21) and (22) has been used to design the current control loops along the two axes. Thus, by adding a PI regulator in the loop control of the d-axis and q-axis rotor currents is realized, as shown in Figure (6.13) [164].

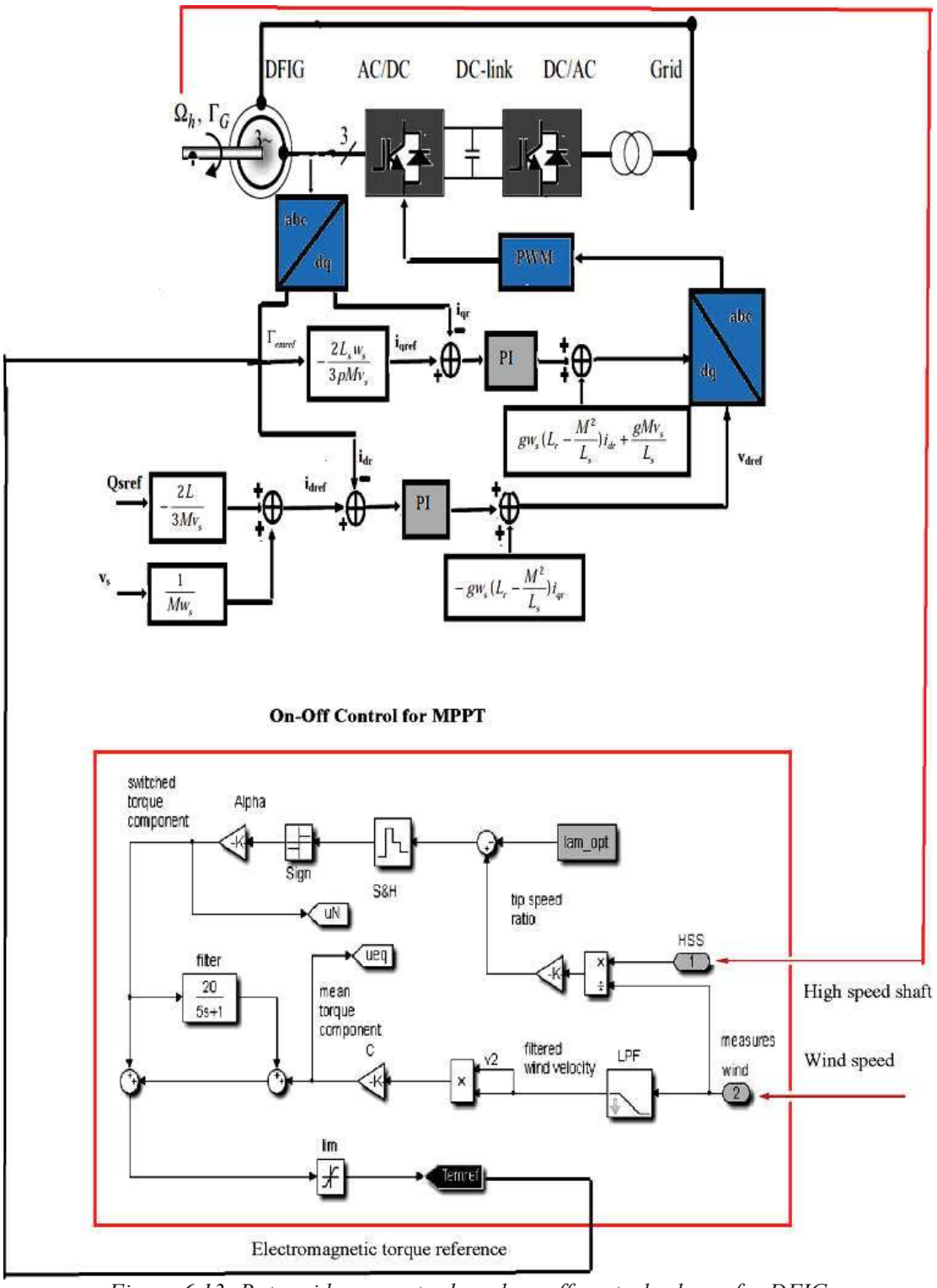

Figure 6.13: Rotor side converter based on-off control scheme for DFIG

6.4.2.3 Inverter and direct bus voltage control: The direct bus voltage is given by the following equation [164]:

$$V_{dc} = \int \frac{1}{c} I_c dt \tag{32}$$

With: $_{Ic} = I_{dc} - I_n$ (33)

With V_{dc} and I_{dc} are the direct bus voltage and current respectively and I_n is the three-phase currents supplied to the grid. The control scheme of the direct bus voltage is presented [156,164] in Figure (6.14). The grid-side converter is used to monitor the voltage of the DC bus capacitor. On behalf of the grid-side controller, the d-axis of the revolving reference frame used for d-q transformation is associated with the actual sequence of the grid voltage. This controller consists of measuring the d-q components of AC currents to be controlled as well as DC voltage. The converter maintains constant dc-link voltage as a reference value during discharge/charge current

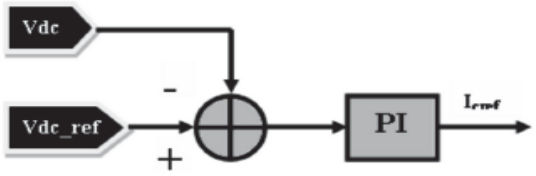

Figure 6.14: Direct bus control scheme

The output DC voltage regulator is fed into the current reference I_{dgc_ref} for the current regulator. Then the current corrector controls the magnitude and phase of the voltage generated by the converter C_{grid} (V_{gc}). The grid side controller is presented [156] in Figure (6.15).

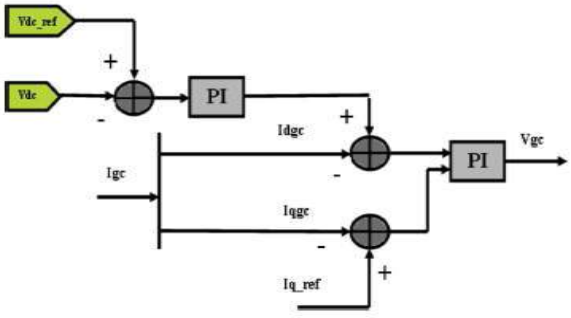

Figure 6.15: Grid side control scheme

6.5 Interpretation and Simulation results

The simulation results in the study state are carried out with MATLAB / Simulink to verify the effectiveness of the considered system using On-Off control for the designed WECS with doubly fed induction generator. Wind speed is typical to assume that the mean value of the wind speed is constant for some intervals. To evaluate the control method aiming at captured power maximisation for DFIG based wind turbine using an On-Off controller, MATLAB is used to carry out the simulation.

6.5.1 MPPT Controller Block

The MPPT block has its input as wind velocity and rotor speed as well as calculates the output as optimal torque reference for maximum power. The developed model of MPPT in SIMULINK workspace is shown in Figure (6.16).

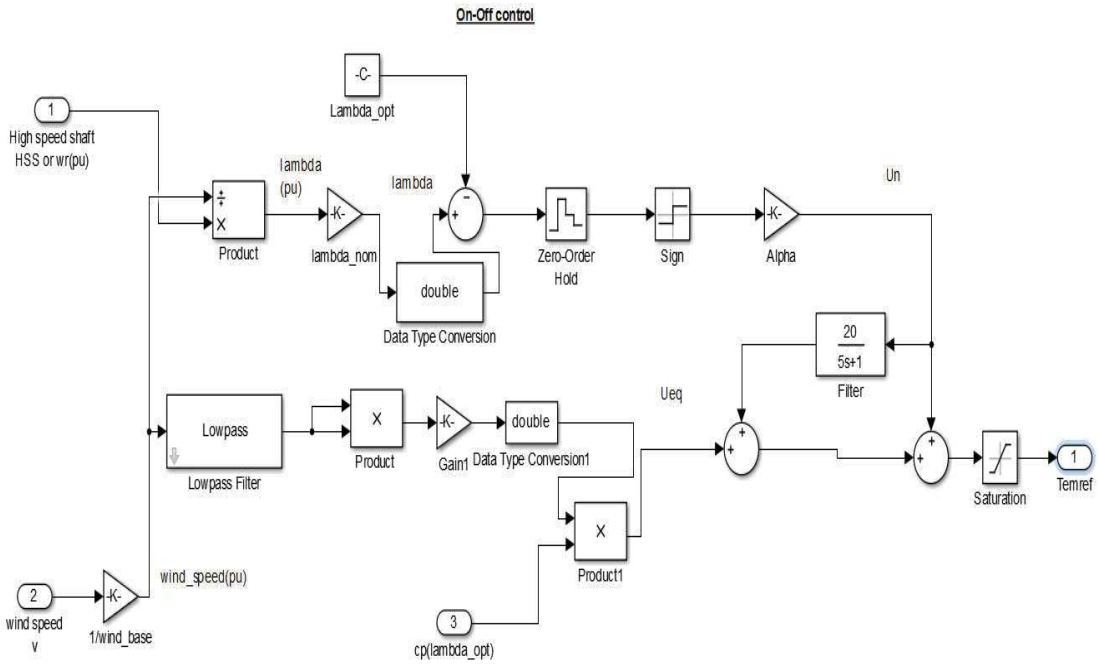

Figure 6.16: MPPT Model for calculating torque reference

The control of the rotor side converter is illustrated in Figure (6.17). The reference i_{qref} is derived from the high-speed shaft Ω_h and measured wind speed V by turning the On-Off controller based maximum power point tracking (MPPT) as shown in Figure (6.18). Also, a current command i_{dref} is derived from Equation (27) to control the reactive power to the required value, as shown in Figure (6.19). Elsewhere; Equations (25) and (26) is used to design the current control loops along the two axes. Thus, by adding a PI regulator in the loop control of the d-axis and q-axis rotor currents is realized.

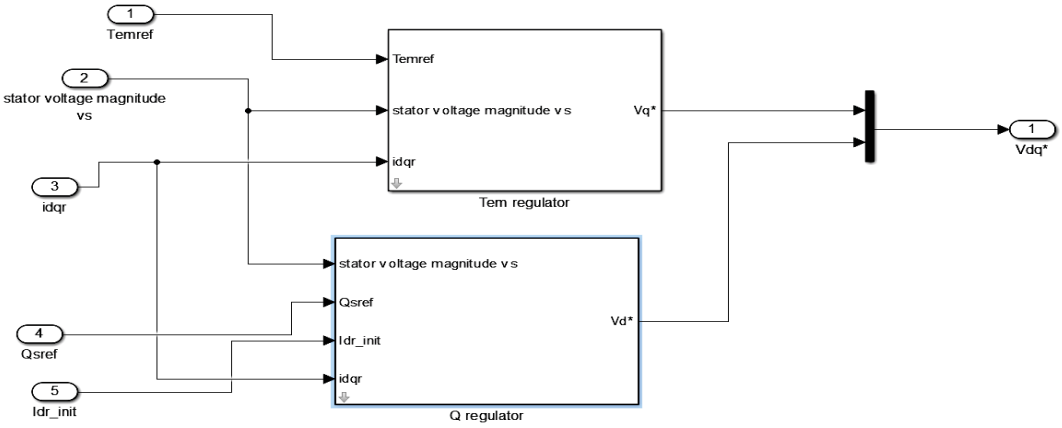

Figure 6.17: MPPT Model for V_{dq} reference

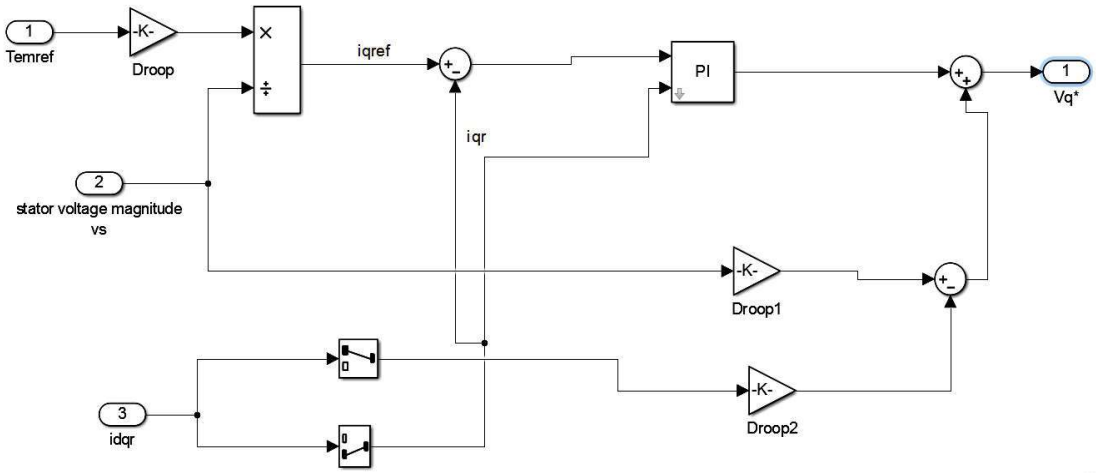

Figure 6.18: MPPT Model for i_{qref}

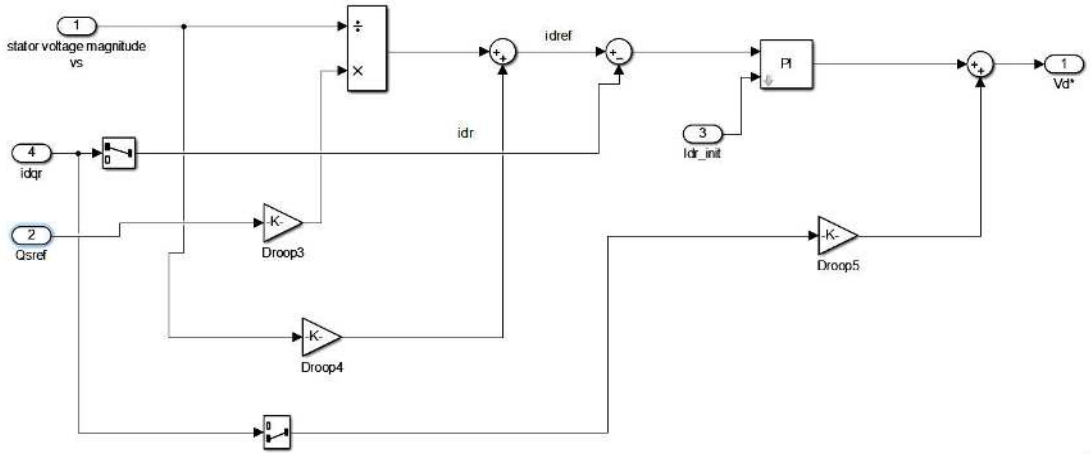

Figure 6.19: MPPT Model for i_{dref}

6.5.2 MPPT based DFIG System model with on-off control scheme Description

The system model, Figure (6.20), can track the torque output from the wind turbine at a given wind velocity. The torque tracked is fed into energy conversion device which converts the available mechanical power into equivalent electrical with the help of a Doubly Fed Induction Generator. It is modeled with a speed control mechanism. The speed control device is achieved with the combination of rotor controllers. The system under study is not only able to track the torque but can maintain a speed of the generator and the coupled turbine shaft to a speed that maximizes the power extracted at a given wind speed. Hence, the outcome is the system that at any time tracks the maximum power from the wind turbine at a given wind velocity. Towards achieving the process, the system modeled works in a three-step operation. In the direction of minimizing the complexity, each block was tested individually, and finally, these blocks are connected to achieve the desired objective. Therefore, based on the sequence of operation, the first operation is performed by the first block the MPPT controller block. The MPPT controller block can generate a reference torque at which the maximum power is extracted from the wind. The second block is a Double fed induction machine which converts the input mechanical power into electrical energy. The double fed induction machine block is constructed of many other

blocks to calculate the rotor currents, stator currents, electromagnetic torque and rotor speed as its output. The third block consists of rotor converter and controller for the rotor circuit converter. The rotor controller has its input as optimal torque from the MPPT block and the actual speed from the generator block. The rotor currents output from the induction generator block also acts as an input to the rotor controller block. The input to the inverter is a DC link voltage which is maintained by a controlled voltage source.

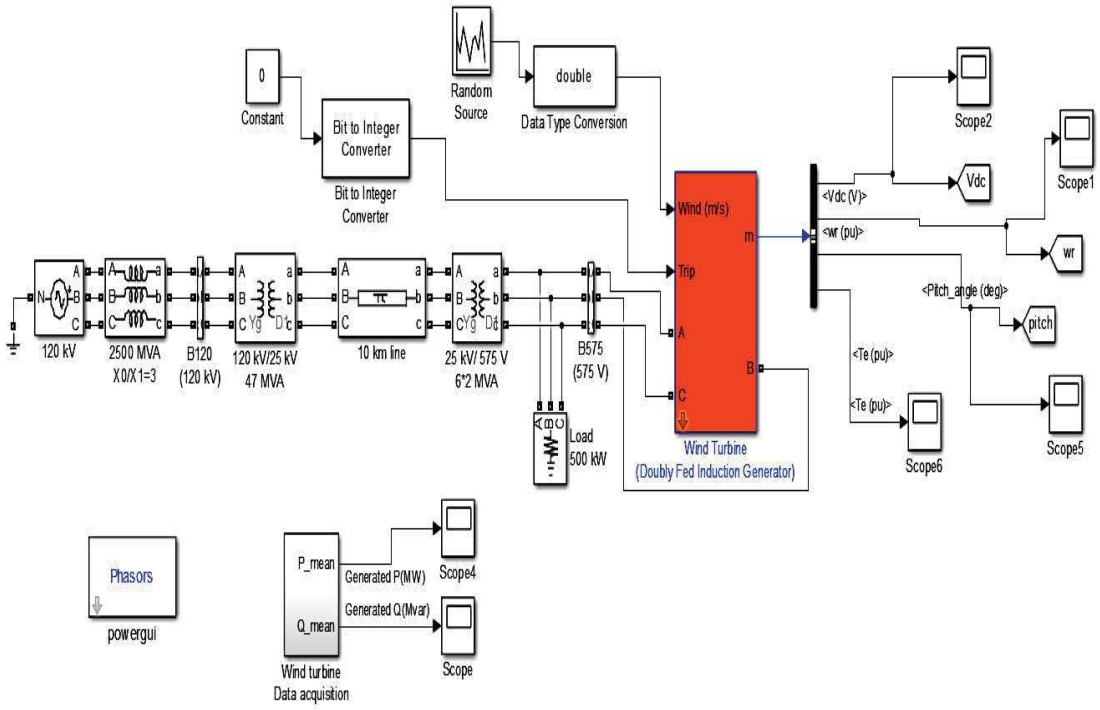

Figure 6.20: DFIG Based Wind Turbine Matlab/Simulink Developed Model

6.5.3 Performance of Rotor Side Controller/Converter

Performance analysis of Rotor side converter includes the observations obtained from the developed model. The view obtained from each block is to be compared with the expected value to check the accuracy obtained from the model. The factor that decides the performance of rotor

side controller is the selection of the gain in the PI controller used in the Speed control loop and Current control loop. For a given wind velocity of 10m/s, the optimal value of torque obtained from the MPPT block is around 25.35 NM, therefore, to get the maximum power the amount of torque should be fixed around 25.35 NM. Along with the torque, the amount of speed should also be at its optimal value. For wind velocity of 10m/s, the value of optimal rotor speed from the MPPT block is 130.9 rad/s, i.e., 1250 R.P.M. Therefore, to obtain the maximum power point the value of generator speed should be maintained at 1250 R.P.M and the torque input should be at 25.35 NM. Also, the value of torque at that speed is calculated by the MPPT block itself. It reads the value of 26.28 NM. Hence the block as a whole is working to track the maximum power from the available wind speed. Towards increase the accuracy of the system, the value of gain constants in the rotor side controller needs to be fine-tuned properly. Hence it can be said that the rotor side controller is indeed decided by the value of the gain constant of the PI controller present in it. Proper selection of this value would result in better effect fast response time.

6.5.4 Simulation Results

The developed model has been tested for various cases with the inbuilt model(conventional model) of Asynchronous machine present in the library of MATLAB. The simulation results are shown in Figures (6.21-6.24) respectively. Figure (6.30) indicates that the dc-link capacitor voltage can be well maintained at 1200 V through the voltage closed-loop control of the grid-side converter. Figure (6.28) is the reactive power. The reactive output power of each wind turbine is almost 0 Var by controlling the rotor-side converter. Figure (6.34) is the actual electromagnetic torque. From Figure (6.34), it can be seen that the value of electromagnetic torque is nearly constant.

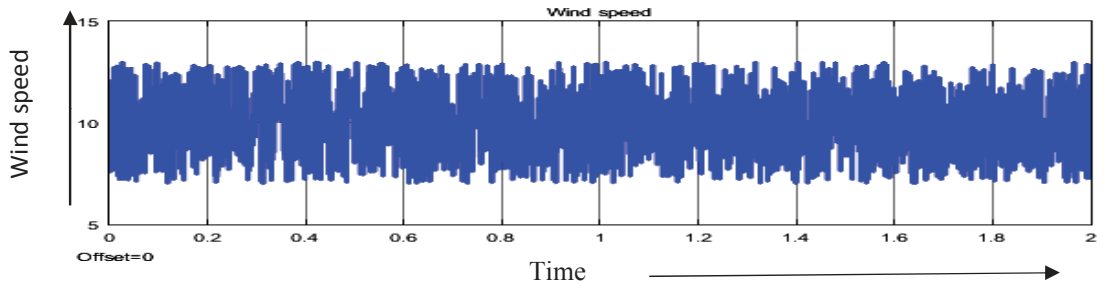

Figure 6.21: wind speed v/s time from developed model

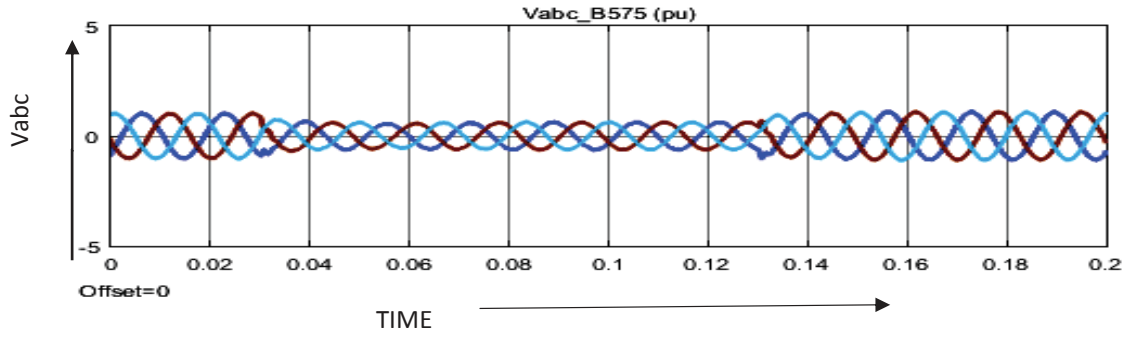

Figure 6.22: V_{abc} v/s time from developed model

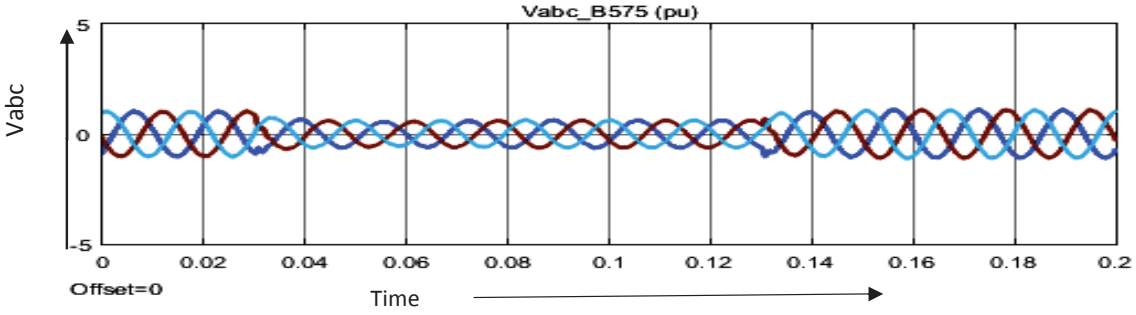

Figure 6.23: V_{abc} v/s time from conventional model

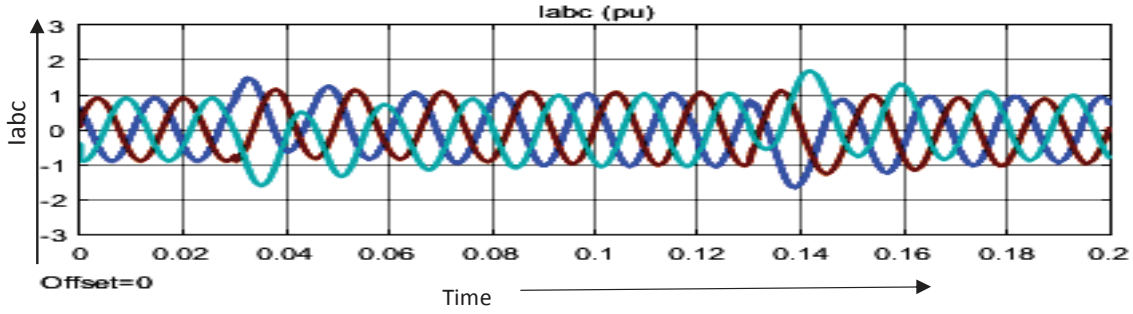

Figure 6.24: I_{abc} v/s time from developed model

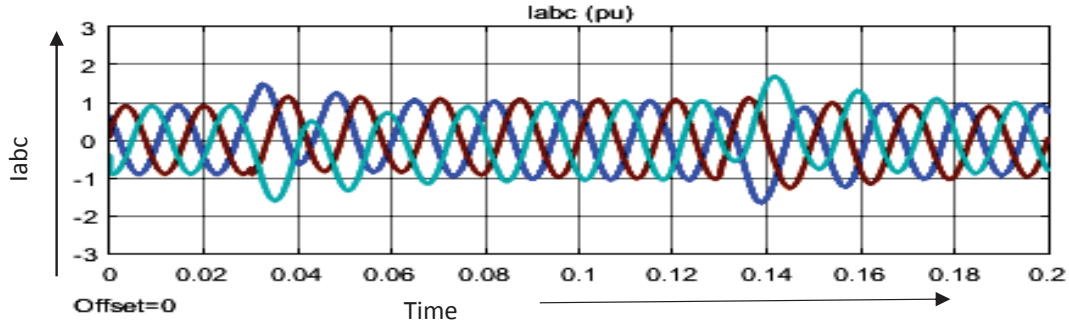

Figure 6.25: I_{abc} v/s time from conventional model

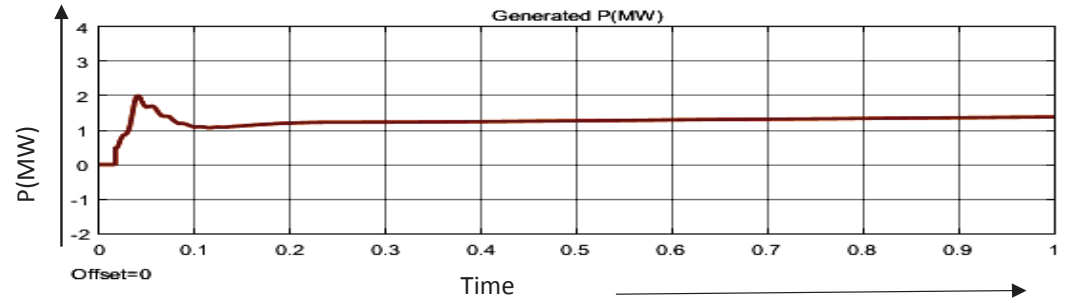

Figure 6.26: Active Power P v/s time from developed model

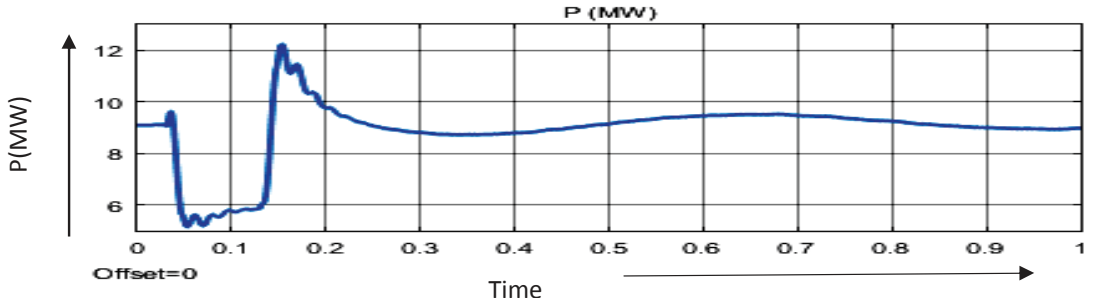

Figure 6.27: Active Power P v/s Time from conventional model

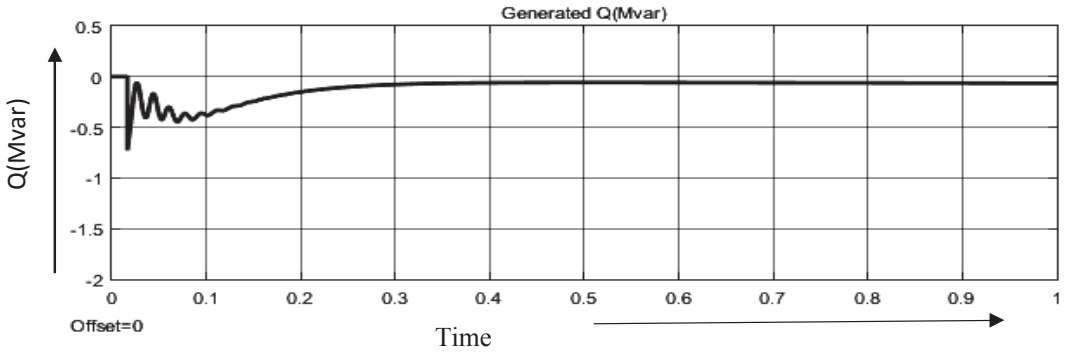

Figure 6.28: Reactive Power Q v/s time from developed model

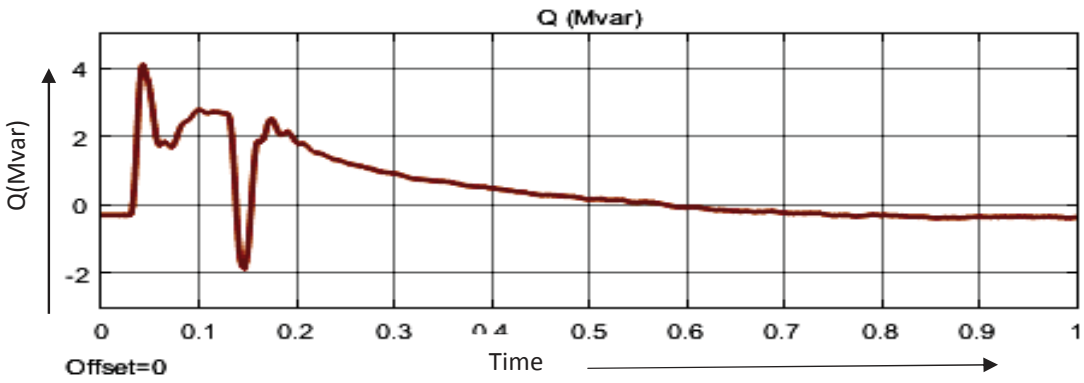

Figure 6.29: Reactive Power Q v/s time from conventional model

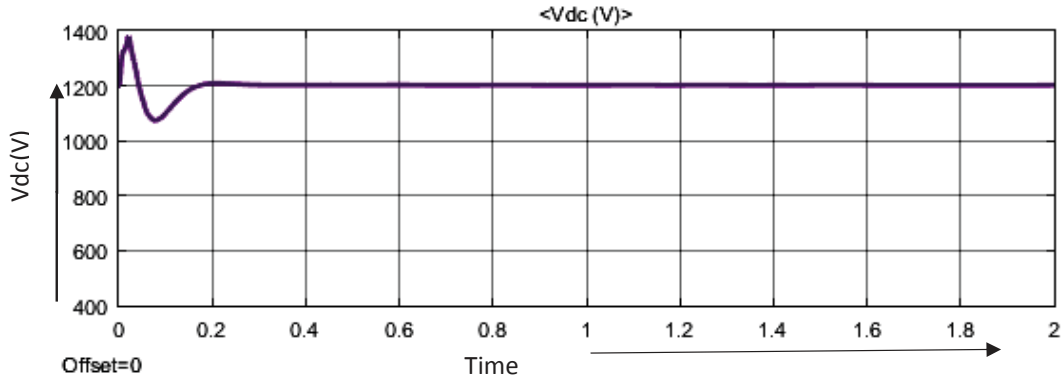

Figure 6.30: DC bus voltage v/s time from developed model

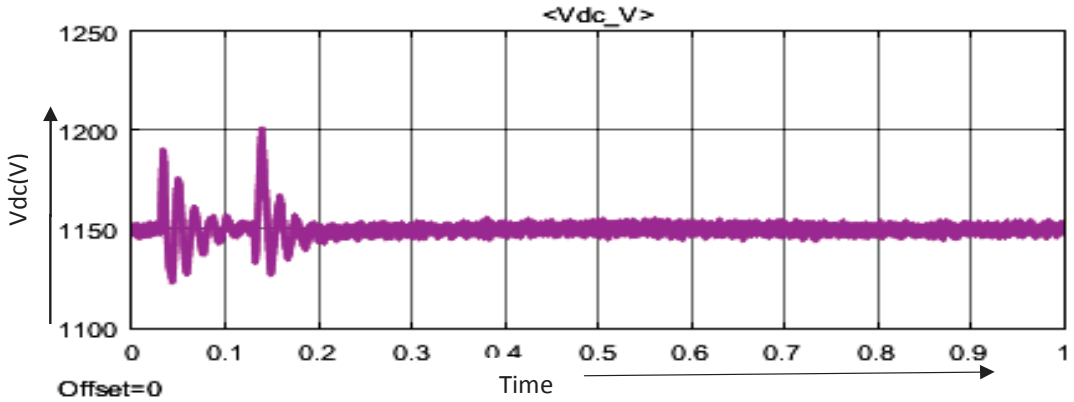

Figure 6.31: DC bus voltage v/s time from conventional model

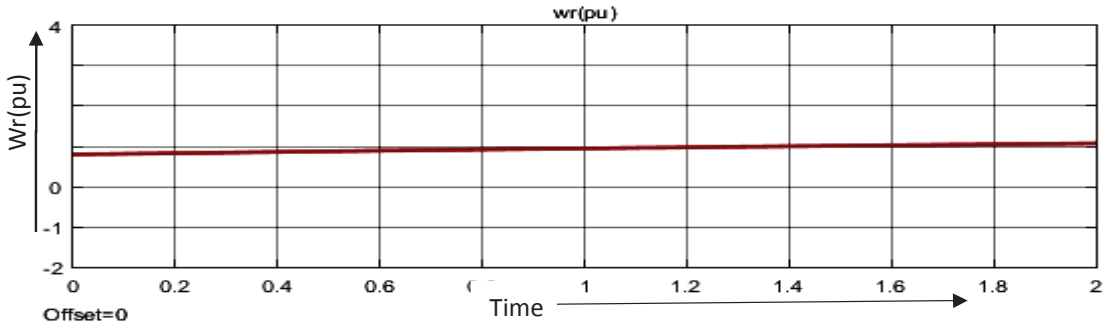

Figure 6.32: Rotor speed v/s time from developed model

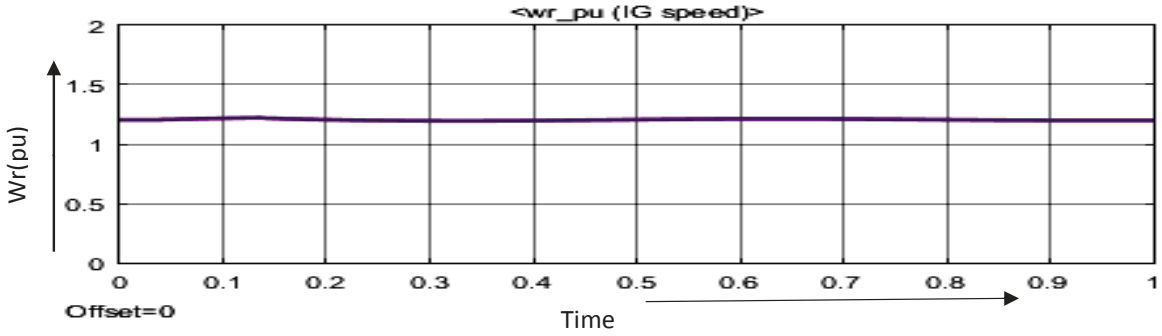

Figure 6.33: Rotor speed v/s time from conventional model

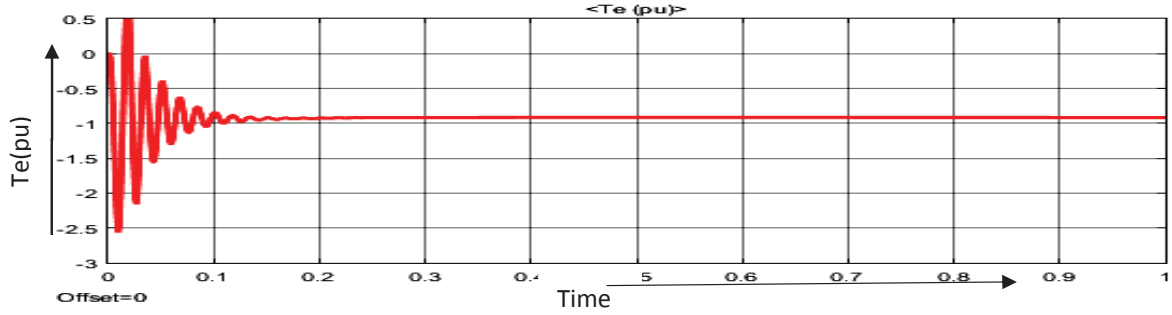

Figure 6.34: Electromagnetic torque v/s time from developed model

Comparing the different set of characteristics of the developed and conventional model Figure (6.22 to 6.34). We can see that the developed model has better characteristics as that of the conventional model.

6.6 Reliability Aspect of Doubly Fed Induction Generator based WT

The high price of the machinery and infrastructure of the wind turbine (WTs) combined with difficulty by Maintenance personnel. The doubly fed induction generators (DFIGs) are extensively applied for wind energy conversion. Their reliability models are significant for risk analysis of WT, which has been thoroughly investigated due to different topology configuration and sensitive reliability data. If high reliability, availability, maintainability, and safety are to be reached, if a bearing or other failure is observed, for example, the repair or refurbishment cost could be Rs. 5000, but, if it is not detected, this could rise to more than Rs. 15000.0 because of security damage to other components. The wind power industry has thus formulated significant Improvements in the field of WT maintenance and repair strategies, employing condition monitoring (CM) integrated within the Supervisory control and data acquisition (SCADA) systems. Fault Detection and Diagnosis, CM and fault detection algorithms are used to allow for early warning of structural, mechanical and Electrical defects, altering wind farm operators to accomplish systematic protection and hence reducing the failure rate. Predictive Maintenance is also used in cycle with preventive maintenance; both are very significant for offshore WTs where the maintenance Personnel operates at sympathy of climate. Different reliability networks have been projected for precise modeling of the WTG system and its sub-systems. Moreover, due to the importance of auxiliary components on reliability calculations, a WTG equipped with an auxiliary mechanical brake has been modeled and studied. The main idea is to divide a WTG into its primary systems and their sub-systems. To examine the reliability of a system, it is required to have the statistical data linked with reliability indices of each component. Here, the information of a Swedish research in a four-year period has been applied. However, in [165] Survey of Failures in Wind Power Systems with Focus on Swedish Wind Power Plants has been

described. After calculating the reliability indices of each system and sub-system, Markov process is used to assess the WTG reliability based on the reliability of its components. The Markov process leads to a model of WTG reliability, which is obtained by solving the differential equations of a stochastic transitional probability matrix. The System reliability (Stationary Markov process) estimates for series, parallel and standby redundant systems in [166,169,170].

6.6.1 Series Systems

Before discussing series systems, first of all, reliability block diagrams should be discussed. For a series systems let's take A, B are subsystem which is followed each other and so on. In the series system, the capability to employ subsystem B depends on functioning state A. Whenever A is not working; the system is down in spite of the condition of Subsystem B. To calculate the system reliability for a continuing process, only need to multiply the estimated reliability of A and B at the time (t). The basic equation used for determining system reliability for the series system is:

$$Rs_{(t)} = R1_{(t)} * R2_{(t)} *\ldots\ldots * Rn_{(t)}\ldots\ldots\ldots\ldots \quad (34)$$

Where: $Rs_{(t)}$ = System reliability for given time (t)

$R1_{(t)}$ - $Rn_{(t)}$ =Subsystem or sub-function reliability for given time (t)

The hazard rate (λ=instantaneous failure rate) for a series system is also a convenient expression.

$$R_s(t) = \prod_{i=1}^{N} \exp(-\lambda_i t) = \exp\{-\sum_{i=1}^{N} \lambda_i\} = \exp(-\lambda_s t) \quad (35)$$

$$\lambda_s(t) = \sum_{i=1}^{N} \lambda_i(t) \quad (36)$$

Therefore, for an ordinary system with three subsystems, each having an estimated reliability of 0.80 (80%) at time (t), the system reliability is calculated as 0.80 × 0.80 × 0.80 = 0.512, or about 51%. As shown in Figure (6.35).

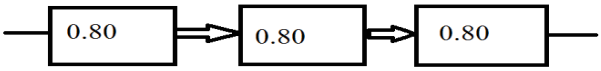

Figure 6.35: Simple Series System

6.6.2 Parallel Systems:

The frequently, design engineers will incorporate redundancy into critical machines. Reliability engineers named these systems to parallel. These systems might be intended as an active parallel system or stand by parallel system. Now block diagram for the simple parallel system is shown in Figure (6.36).

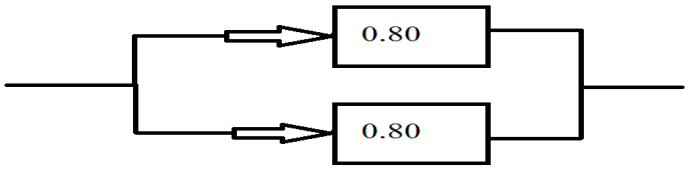

Figure 6.36: Simple parallel system

To estimate the reliability of an active parallel system, when both machines are in operation, then the following equation is taken as:

$$R_s(t) = 1 - [(1-R_1(t)) * (1-R_2(t)) * \ldots\ldots * (1-R_n(t))] \quad (37)$$

Where: Rs (t) = System reliability for given time (t)

R1 (t) – Rn (t) = Subsystem or sub-function reliability for given time (t)

$$R_s(t) = 1 - \prod_{i=1}^{N} \{1 - R_i(t)\} \quad (38)$$

System for two blocks system

$$R_s = 1 - [1 - \exp(-\lambda_1 t)][1 - \exp(-\lambda_2 t)] \quad (39)$$

The simple parallel system in giving an example with two components in parallel, each having a reliability of 0.80, has a total system reliability of 1- (0.2 × 0.2) = 0.96. So, the system reliability extensively enhanced.

6.6.3 Standby Redundant Systems:

A system is called a redundant standby system when some of its units are inactive till that is required service by a sensing and switching device (SS).For simplicity, let's consider a situation where only one unit operates actively, and the others are on standby. The redundant standby system is as shown in Figure (6.37).

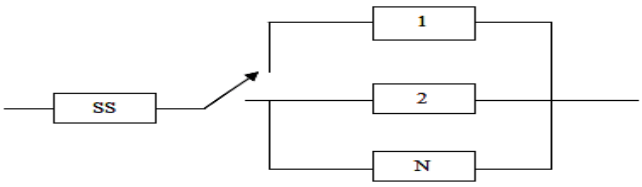

Figure 3.37: Standby Redundant System

In this arrangement, unit 1 continually operates until it fails. The sensing and switching device recognizes a unit failure in the system and switches to another unit. This procedure continues till every standby unit has failed, for that case, the system is considered failed. Since units 2 to N do not operate regularly (as a case inactive parallel systems) it would expect them to fail at a much slower rate. Because the failure rate for components is usually lower when the components are operating which are idle or dormant.

Mathematically, the reliability function for a two block (unit) standby device according to this definition can be obtained as:

$$R_s(t) = R_1(1) + \int_0^{\infty} f_1(t_1)\,dt.R_{ss}(t_1).R_2'(t_1).R_2(t-t_1) \tag{40}$$

Here f1 (t_1) is the pdf (probability density function) for the time to failure of unit 1. Rss (t_1) is the reliability of the sensing and switching device. R'2 (t_1) is the reliability of unit 2 in the

standby mode of operation, and R2(t-t1) is the reliability of unit 2 after it started to operate at time t1. Let's consider a case where time to failure of all units follows an Exponential distribution,

$$= \exp(-\lambda_1 t) + \frac{\lambda_1 \exp(-\lambda_2 t)}{\lambda_1 + \lambda_{ss} + \lambda_2^{'} - \lambda_2}\{1 - \exp[-(\lambda_1 + \lambda_{ss} + \lambda_2^{'} - \lambda_2)]t\} \quad (41)$$

$$= \exp(-\lambda_1 t) + \frac{\lambda_1 \exp(-\lambda_2 t)}{\lambda_1 + \lambda_{ss} + \lambda_2^{'} - \lambda_2}\{1 - \exp[-(\lambda_1 + \lambda_{ss} + \lambda_2^{'} - \lambda_2)]t\} \quad (42)$$

For the particular case of perfect sensing and switching and no standby failures,

$\lambda_{ss} = \lambda'2 = 0$

$$= \exp(-\lambda_1 t) + \frac{\lambda_1 \exp(-\lambda_2 t)}{\lambda_1 - \lambda_2}\{1 - \exp[-(\lambda_1 - \lambda_2)]t \quad (43)$$

$$= \exp(-\lambda_1 t) + \frac{\lambda_1}{\lambda_1 - \lambda_2}\{\exp(-\lambda_2 t) - \exp(-\lambda_1 t)\} \quad (44)$$

6.6.4 Historical Data Analysis of DFIG based WT

As stated before, a wind unit is divided into two system, sub-systems and different system components. It is required to know the reliability parameters for each of these elements. Data obtained from wind power plants are available in literature and are used here. There is the possibility of probable fault detection at point P. whenever a failure is not mitigated; the deterioration continues until functional breakdown at stage F; then the time between P and F is the period during which the fault can be avoided. It is demonstrated that failures can be predicted with reasonable accuracy before they occur by employing a CM system. Figure (3.38) shows the Deterioration Failure Leading up to the Fault, called P–F Curve.

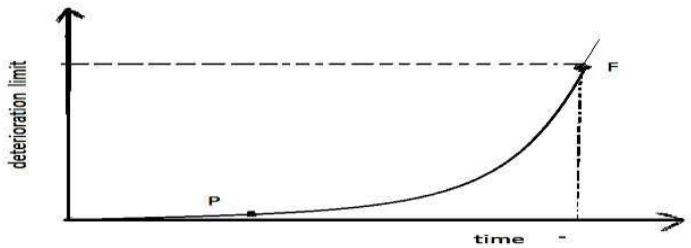

Figure 6.38: P–F Curve

The life of a new WT is around 20 years, and WT failures are common to follow a bathtub curve as shown in Fig. 3.5. Here high rates of failure will be observed for both early on (period of early failures) and towards the end of life (period of wear out) but within lower rate, the middle period (use full life period) are presented in [167,169,170]. Wind turbines are operating in their periods of early failure and ones in their periods of usage. They failed to find any data for wear out periods because WTs were comparatively new and lost reliability which tends to be taken out of service before wear out. However early failure Period appears to be reaching long. Now bathtub curve is as shown in Figure (3.39).

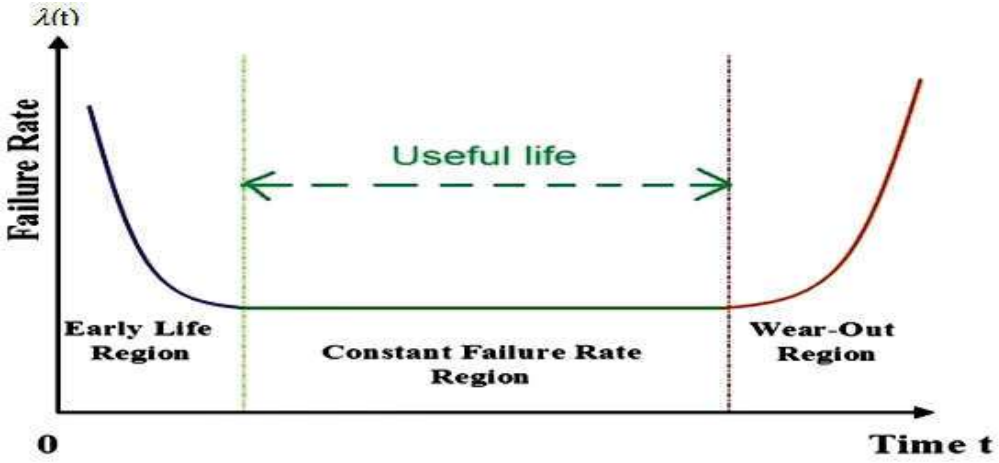

Figure 3.39: Bath Tub Curve

However, average failure rate usually described the number of failures per turbine per year. Now the failure rate is formulated as follows:

$$f = \frac{\sum_{i=1}^{I} N_i}{\sum_{i=1}^{I} X_i T_i} \tag{45}$$

Where f is the failure rate [failures per turbine per year], Ni number of failures that occurred during the time interval T_i, Ti time interval (I in total of 1year each one), Xi number of WTs

reported for the time interval T_i and i is (1, 2… I), years. In similar downtime is the time during which a WT is not operating because of a fault, typically comprised of time for

- Diagnosing the failure (in the case of non-condition monitoring systems)
- Collecting repair apparatus along with standby part
- Getting at the mechanism
- Repairing and restarting the WT

6.6.5 DFIG based WT Components

Prime apparatus of reliability network for a DFIG based WT are explained in previous chapter 4. Figure (3.40) shows the typical DFIG based WT along with its apparatus.

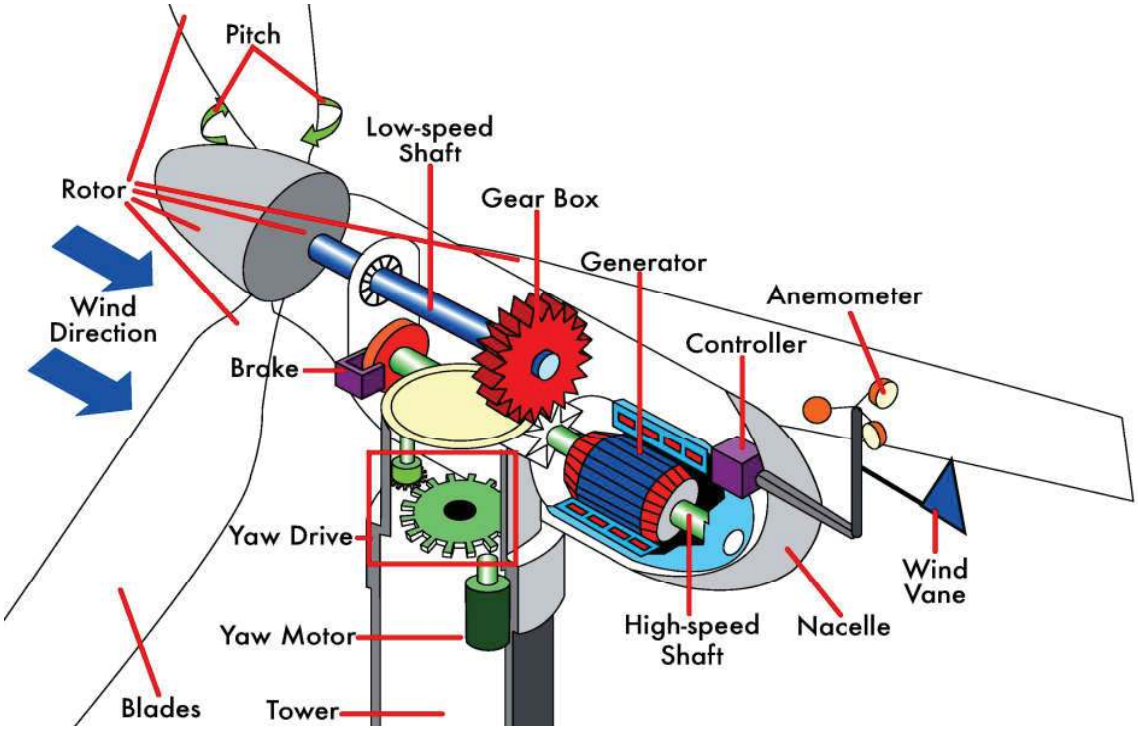

Figure 3.40: Module of DFIG based Wind Turbine

Rotor: it is composed of blades and a hub. Blades absorb the wind energy and transmit it to hub.

Pitch motor: wind turbines equipped with pitch control, the blades turn to the wind direction according to Maximum Power Tracking (MPT).

Mechanical brakes: The connection shaft between gearbox and generator is equipped with mechanical brake systems which are disc type brakes.

Gearbox: The purpose of the gearbox is connected to the low-speed axis at one end and to electricity generator at the other end, to increase the low rate of rotor turn appropriately.

Generator: Generators used in DFIG based wind turbines are of induction type.

Anemometer: An anemometer is a apparatus that measures wind speed as well as wind pressure.

Controllers: it has several electrical and mechanical controllers for controlling and coordination of different parts of the DFIG.

Sensors: In each DFIG based WTG, sensors of different types are used to provide information such as wind direction, wind intensity, rotor speed, voltage, current, output power, heat indicators, gearbox oil, hydraulic system gauges and so on.

Nacelle: Nacelle holds the main components of a wind turbine like gearbox, generator, shaft and other parts. The rotor is located at the Nacelle head while sensors for wind speed are placed at the end.

Yaw motor: This system employs two or more electric motors for rotating the nacelle in the wind direction. That's controlled from a central control room which recognizes the wind direction based on data from sensors and sends the necessary commands to motors.

Tower: Nacelle with blades is mounted on a tower. In general, the higher tower is better because wind speed increases with height from the ground. In a 2MW generation, DFIG based wind turbine has the tower height is about 50 to 80 meter.

Converters: A DFIG based WT uses two converters namely grid side and rotor side. DFIG can operate both in super-synchronous and sub-synchronous modes requiring the converter to work bi-directionally.

6.7 **DFIG Based WT's Sub-systems**

For DFIG based WT Reliability models analysis, few major elements were considered, whereas for new elements series reliability models have been applied. However, to study the reliability of a wind turbine, a precise reliability model must be designed based on all comprising elements and relations of each component with grid as well as failure and repair rate of each component, to prevent the complication of mentioned model.

6.7.1 DFIG based WT Component Failure Analysis

Several studies have been carried to gather WTG reliability data. The data are presented in different configure (such as; failure, downtime distributions (%), failure rates as failures per turbine for every year, downtime while hours went for each component for every WT per year) from different locations. Along with weather conditions and types of WTs with a range of operational life [166]. Among these, it shows that weather and location are factors in the reliability of the WTs due to the wind speed. Significant cross-correlation exists between the failure rate and the climate condition; hotness along with moisture was more efficient than the wind speed. However, to study the reliability of a wind turbine, a precise reliability model must be designed based on all comprising elements and relations of each component with grid as well as failure and repair rate for each element. To prevent complexity in the mentioned model, here a wind unit is divided into three systems [167]. Each part is subdivided into smaller sub-systems:1. Electrical system, 2.Mechanical system, 3.Structural system, The DFIG wind unit subsystems are as shown in Figure (6.41).

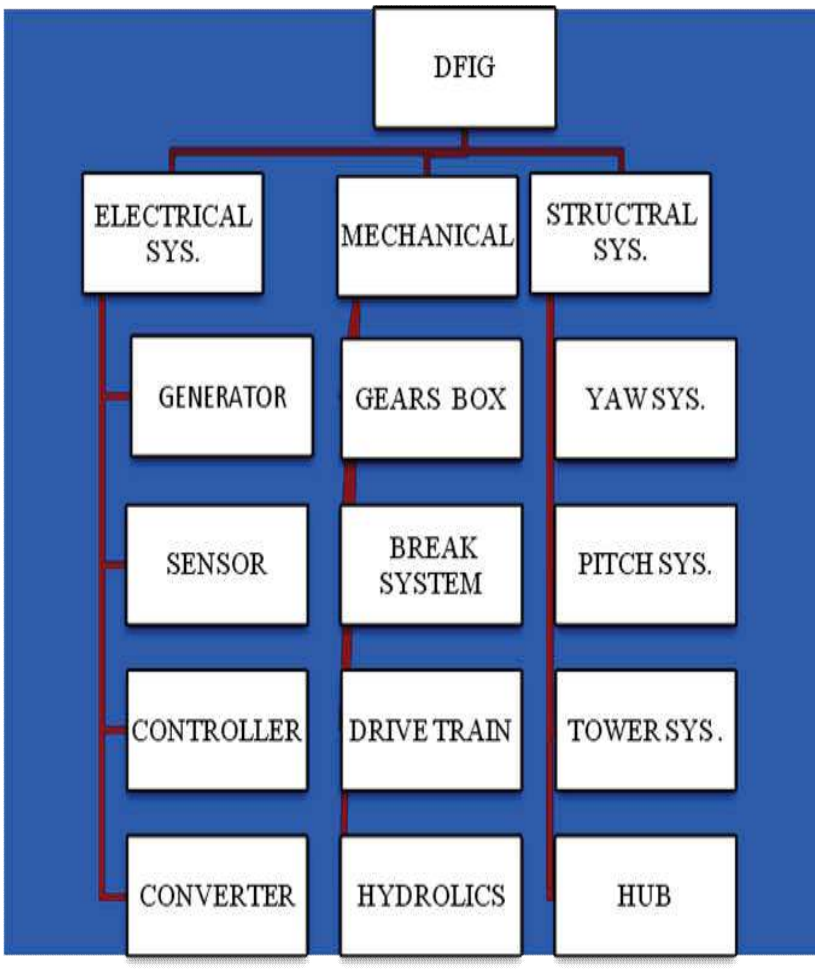

Figure 6.41: DFIG based WT Unit Sub-Systems

Three main parts, electrical, mechanical and structural are studied separately in the developed RBD. Apparently, the system could full fill its regular job components function normally. Even though sub components operate electrically and contain electrical sub components but the structural subsystem and got different positions in the overall RBD in evaluation from the electrical subassemblies due to their close interaction with the hub, the critical structural

component, and also because of the difference between their operation and that of the other electrical Components. In the case of pitch and yaw malfunctioning system may not work optimally since the maximum amount of wind power cannot be fascinated, but still, the system could continue its operation in a derated state. That's why these two subcomponents are considered as parallel with the other blocks in the overall RBD. Which is shown in Figure(6.42) the Normally Closed (NC) switches would be opened if any serious malfunctions in the operation of the main route of the RBD take place; while probably trouble sub components lead the system to operate in the derated state.

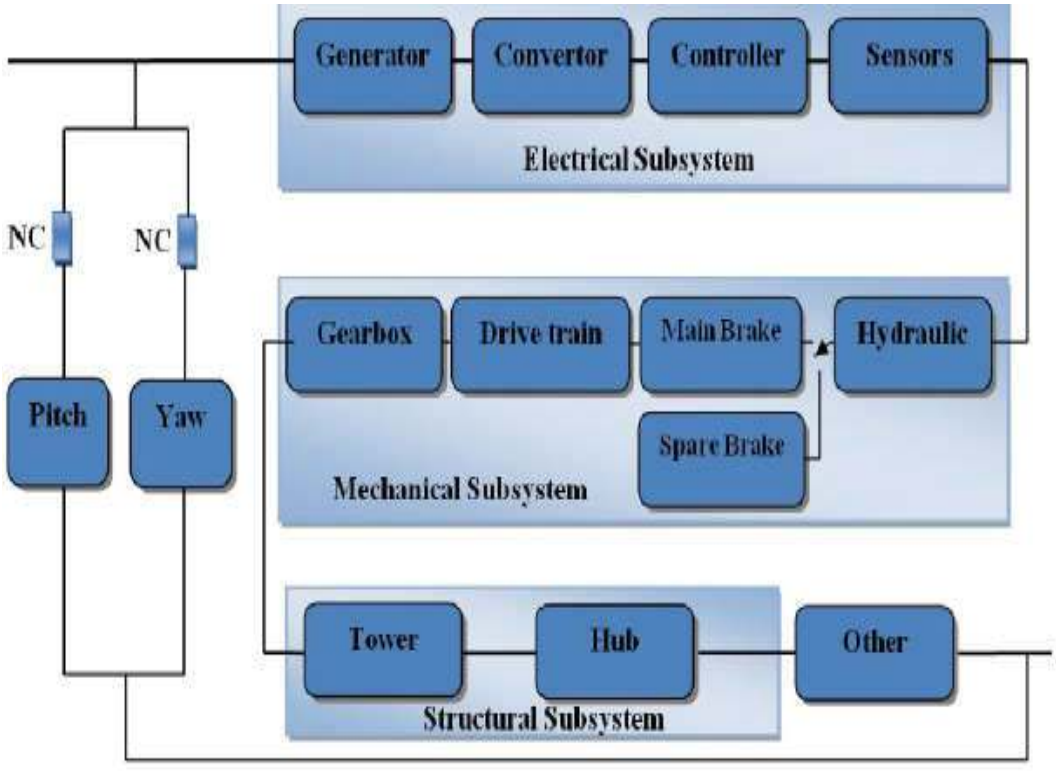

Figure 6.42: General RBD for the DFIG system

Finnish wind farm complete failure and downtime data [168] is shown in Table (6.1&6.2).

Table 6.1: Finnish wind farm detailed failure and downtime data

Component	Total downtime per component [h]	Average downtime per year [h/r]	Average downtime per year per turbine [h/yr/turbine]	Distribution of downtime [%]	Total number of failures per component[n]
Blade /pitch	17916	3583	50.3	21.2	70
Generator	3686	737	10.4	4.4	30
Electric system	5427	1085	15.2	6.4	38
Control system	1431	286	4.0	1.7	34
Drive train	0	0	0	0	0
Sensors	1727	345	4.9	2.0	41
Gears	27706	5541	88.0	32.8	46
Mechanical brakes	2330	466	6.5	2.8	16
Hydraulics	9652	1930	30.6	11.4	112
Yaw system	5495	1099	15.4	6.5	36
Structure	5524	1105	15.5	6.5	31
Other	1739	348	4.9	2.1	22
Unknown	1739	347	4.9	2.1	12
Total	84428	347	237.2	100	491

Table 6.2: Finnish wind farm detailed average failure as well as downtime data

Components	Average failure Number per year [n/yr]	Average Number of failure per year per turbine [n/yr/turbine]	Distribution of failures [%]	Average downtime per failure [h/failure]
Hub	0.6	0.01	0.6	20
Blade /pitch	14.0	0.20	14.3	266
Generator	6.0	0.08	6.1	123
Electric system	7.6	0.11	7.7	143
Control system	6.8	0.10	6.9	42
Drive train	0	0	0	0
Sensors	8.2	0.12	8.4	42
Gears	9.2	0.15	9.4	602
Mechanical brakes	3.2	0.04	3.3	146
Hydraulics	22.4	0.36	22.8	86
Yaw system	7.2	0.10	7.3	153
structure	6.2	0.09	6.3	178
Other	4.4	0.06	4.5	79
Unknown	2.4	0.03	2.4	145
Total	98.2	1.38	100.0	172

The data used in this chapter are gathered from a Finnish wind farm, narrating the operation of the field. The data corresponds to the most detail sub-component of the system and could be used for a comprehensive study; although it's significance mention that main sub components are analyzed in this chapter, and their particular sub components statistics (for example gearbox and lubrication) are collective in the major subcomponents. The statical and interpretive component summary of WTs is listed in Table (6.3). while detailed data containing failure and repair rates are shown in Table (6.4). The distribution of failure rate and downtime is given in [168] as shown in Figure (6.43&6.44).

Table 6.3: Summary of the Statics and Critical Component

Average number of turbines	71.2 turbines
Average number of failures	1.38 times a year
Average downtimes	237 hour per year, 172 hours per failure
Highest failure rates	Hydraulics, Pitch /Blades, Gearbox
Highest downtimes	Gearbox, Pitch/Blades, Hydraulics
Longest downtimes	Gearbox, Pitch/Blade, Tower

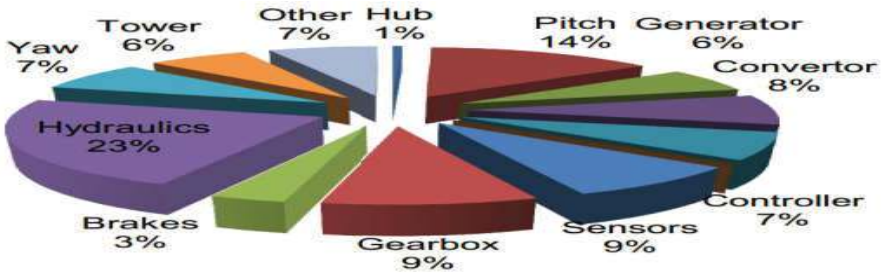

Figure 6.43: Distribution of Failure Rate

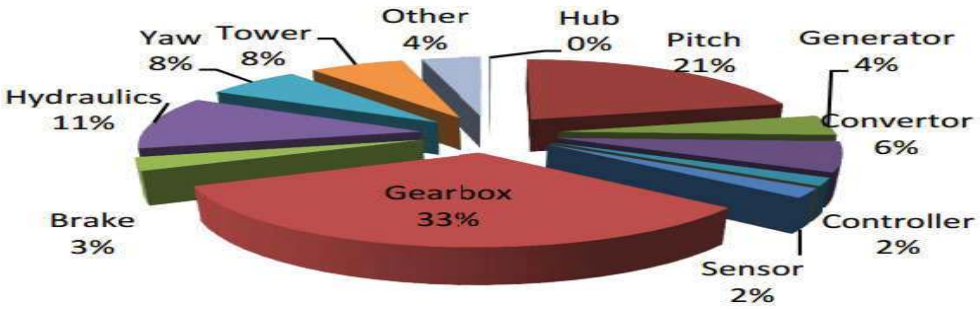

Figure 6.44: Distribution of Downtime

6.7.2 Electrical subsystem

The controller, sensor, and generator along with converter block are presented in series in the model since any malfunction in their process leads the entire system towards fail. For the meantime, its significance to be emphasizing that the blocks being in series in the reliability model are theoretically dissimilar from their constituting series electrically. According to, the electrical subsystem equivalent failure and repair rate could be calculated by using equations (38) & (39) (usable for systems containing series components only), where *I* represent the elements number

$$\lambda_{eq} = \sum \lambda_i \tag{46}$$

$$MTTR_{eq} = \frac{1}{\mu_{eq}} = \frac{\sum \frac{\lambda_i}{\mu_i}}{\sum \lambda_i} \tag{47}$$

6.7.3 Mechanical Subsystem

The gearbox, drivetrain, and hydraulics along with brake compound are presented as series of the mechanical blocks. It is general that some wind turbines contain a first disc brake as well as a spare brake which is mainly scissor typed or in rare cases air typed. The spare brake modeled in this chapter is assumed to have half the failure rate of that in the first brake; however, it has similar repair rate like as first brake. According to

$$R_{brake}(\mathrm{t}) = \mathrm{R}_{1}(\mathrm{t}) + \mathrm{R}_{2}(\mathrm{t}) \tag{48}$$

Where R_1 (t) is the probability of the first brake implemented accurately at time t, while R_2 (t) is the probability of the primary brake functioning accurately at time t_1, along with the spare one towards operating from t_1 to t, while $t_1 <$ t. Thus:

$$R_1(\mathrm{t}) = e^{-\lambda_1 t} \tag{49}$$

$$R_2(\mathrm{t}) = \int_{t_1=0}^{t} \lambda_1 e^{-\lambda_1 \cdot t_1} e^{-\lambda_2 \cdot (\mathrm{t}-\mathrm{t}_1)} dt = \frac{\lambda_1}{\lambda_1 + \lambda_2} [\mathrm{e}^{-\lambda_2 t} - \mathrm{e}^{-\lambda_1 t}] \tag{50}$$

Where λ_1 represents a failure rate of the first brake Furthermore, λ_2 is a spare brake.

Considering the results of equations 11, 12, 13, $MTTF_{mech}$ and $\lambda_{Mech.}$ could be calculated as

Follows, whereas similarly MTTRmech and λ_{MTTR} is also derived from these Equations.

$$MTTF_{Break} = \int_{0}^{\infty} R_{Break}(\mathrm{t})\,\mathrm{dt} = \frac{1}{\lambda_{Break}} = \frac{1}{\lambda_1} + \frac{1}{\lambda_2} \tag{51}$$

$$\lambda_{Mech.} = \lambda_{Break} + \lambda_{Hydrolic} + \lambda_{Gear} + \lambda_{Drvtrn} \tag{52}$$

6.7.4 Structural Subsystem

Two main blocks are included in this subsystem, the tower and the hub; which are put in series in the RBD (reliability body diagram) due to their principal role in the WECS operation. The pitch and yaw apparatus are supposed to be chosen parallel block in the RBD since the malfunctioning leads the system to the "derated" state and not to "Fail." similar to Equations

$$\lambda_{strc} = \lambda_{tower} + \lambda_{hub} \tag{53}$$

$$\mu_{strc} = \frac{\lambda_{tower} / \mu_{hub} + \lambda_{hub} / \mu_{hub}}{\lambda_{tower} + \lambda_{hub}} \tag{54}$$

However, the equivalent failure rate (λ_{eq}) and repair rate (μ_{eq}) for electrical, mechanical along with structural systems have been evaluated by data [168], which is shown in Table (6.4).

Table 6.4: Blocks for failure and repair rates

Block	Electrical	Mechanical	Structural
λ_{eq}	0.41	0.52	0.1
μ_{eq}	6.36	34.64	1.69

So that straight forward comprehensive pooling is impossible. Following observations have been done on a selection of recent studies.

- Stationary Markov process is used to compute the reliability of the whole DFIG based WT system based on the reliability of its subsystems. The proposed model is flexible since the failure rate and the mean time to repair rate can be calculated for different operational conditions and specifications based on DFIG technology.
- The reported failure rates of hubs, generators, sensors, brakes, yaw systems, and structure, do not vary very much between different studies.
- Blades, control systems, and electrical system are often cited in correlation using failure rates; gearboxes, generator sand blades feature most in consideration of downtime.
- Most problematic components such as gears, blades or hydraulics with combinations of failure rate along with downtime per failure that outcome in higher downtime (hours lost per turbine per year)

The publications from this part of the thesis work are as follows;

- Rahul Gangwani, **Om Prakash Bharti**, R.K. Saket, Shiv Lal, "*On-Off control based maximum power point tracking of wind turbine equipped by DFIG connected to the grid*", **Advances in Power Generation from Renewable Energy Sources (APGRES 2017),** December 22-23, 2017, Govt. Engg. College, Banswara, Rajasthan, pp: 162-168, 2017.
- **O.P. Bharti,** R.K. Saket, S.K. Nagar, *"Reliability Analysis of DFIG Based Wind Energy Conversion System",* **International Conference on Renewable Energy Technology** (ICRET-2017), January 22-24, 2017, Thammasat University, Klong Luang, Pathumthani, **Bangkok, Thailand**, pp: 313-317, 2017 {BEST PAPER AWARD}.
- **Om Prakash Bharti,** R. K. Saket, S.K. Nagar, *"Reliability assessment and Performance analysis of DFIG based WT for wind energy conversion system"* **International Journal of Reliability and Safety**, from Inderscience Publishers, Under Review 2018. SCOPUS Indexed Journal.

6.8 Conclusion

Wind Energy market is rocketing high at present. A lot of research and developmental works have been going on in the field of wind energy to find the optimal ways to harness the available power. A concept of MPPT has been proposed to achieve the goal of tracking maximum power at a given wind velocity. To perform the MPPT from the wind system, the MPPT block in coordination with the rotor control block acts to maintain the torque to the value that is optimum for extracting the maximum power output from it. The energy conversion device which is used in wind turbine systems is Doubly Fed Induction Generator. Therefore, a doubly fed induction generator is modeled as an energy conversion device. The modeling included the verification of developed model with that of the generator present in the library of the MATLAB/ Simulink. The results are better than of the model in the MATLAB library. Further to achieve a double-fed induction generator the modeled generator has incorporated with rotor side converters and controllers. The results obtained showed that the system could perform well at average wind speeds while the results are inconsistent with that of expected values at lower and higher wind speeds. Hence at average wind speed, the rotor side controller changes such that to alter the torque to the optimal value generated by the MPPT controller. On the other hand the recent reliability analysis of the DFIG is described in this chapter. The stationary Markov process is used to compute the reliability of the whole DFIG based WT scheme with subsystems. The proposed model is flexible since the failure rate and the mean time to repair rate can be calculated for different operational conditions and specifications based on DFIG technology.

The Chapter 7 finally summarizes the present thesis and includes the conclusions of all the chapters. Moreover, chapter 7 is also pointed out the scope of future work.